Analysis of Electromagnetic and Quantum Effects on Low Dimensional MOS Transistors

by

Víctor Hugo Vega González

A Dissertation
Submitted to the Program in Electronics Science,
Electronics Department
in partial fulfillment of the requirements for the degree of

DOCTORATE IN ELECTRONICS SCIENCE

at the
National Institute for Astrophysics, Optics and Electronics
June 2014
Tonantzintla, Puebla

Advisors:
Dr. Edmundo Gutiérrez Domínguez
Dr. Fernando Guarín

ABSTRACT

Overall, this work introduces experimental and theoretical work that offers the reader an alternative perspective of looking at 28 nm MOSFET electrical performance and modeling.

Chapter 1 introduces an alternative way to produce a negative differential resistance (NDR) effect that is achieved by the non-conventional biasing of a regular 28-nm n-type Metal-Oxide-Semiconductor Field-Effect Transistor (n-MOSFET). It has a controllable peak-to-valley current ratio (PVCR) that goes from about 3.0 up to a room-temperature value of 5.5, which is above the record of 5.3 previously reported on silicon heterostructures [1]. Two bipolar mechanisms working in parallel are demonstrated to occur inside the n-MOSFET, one at the surface and other in the bulk. Thermally activated electrons are injected into the gate contact through the drain-gate overlap, a situation that leads the transistor to the flat-band condition, blocking the surface conduction channel and triggering the NDR effect. I proposed a simple analytical model that correlates very well with experimental data.

Chapter 2 provides a general perspective of the theoretical approaches that can lead to the determination of the charge current through a nano-scaled system from a full quantum mechanical perspective. It exposes the amount of information that, in principle, can be obtained from any physical system and the complications that arise in the determination of the current. The more realistic but still very difficult statistical quantum mechanical approach is briefly presented afterwards. Finally, the Landauer formalism is established as a series of assumptions that render a close-form expression for the current in terms of the probability of transmission.

An analogy between the time-independent Maxwell and Schrödinger equations is developed in Chapter 3. It is applicable to two-dimensional systems with wave-guide (lead) boundary conditions. On the lead boundaries, the third-order boundary conditions for the electric field reduce to the normal derivative of its z-component, adopting the same form of the equivalent boundary conditions for the Schrödinger equation. The total energy and position-dependent potential energy are included in the set of quantities that have an equivalent electromagnetic parameter.

Standard electromagnetic analysis methods were applied to determine the wave function and transmission probability of phase-coherent quantum electron devices including a tunneling structure. The Schrödinger equation was solved via the Quantum Transmitting Boundary method for comparison with the electromagnetic simulations.

The Non-Equilibrium Green's Function (NEGF) formalism is the most prominent theoretical approach when it comes to quantum transport analysis, modeling and characterization of nano-scaled systems. In fact, the NEGF formalism is considered the quantum version of the Boltzmann transport theory. Based on NEGF formalism, a systematic analysis of different multiport nanostructures modulated by the action of a magnetic field is introduced in chapter 4.

RESUMEN

En este trabajo se presenta una visión alternativa sobre el comportamiento eléctrico experimental y el modelado de transistores MOS de la tecnología de 28 nanómetros.

En el capitulo 1 se presenta una forma alternativa para producir un efecto de resistencia negativa el cual se logra a través de la polarización no convencional de un transistor de efecto de campo convencional tipo (n-MOSFET). Este efecto tiene una relación de corriente pico que va de 3 a un valor a temperatura ambiente de 5.5, aproximadamente, el cuál está por arriba del valor record reportado para dispositivos de resistencia negativa basados en hetero-estructuras [1]. Se demuestra la presencia de dos mecanismos bipolares trabajando en paralelo dentro del n-MOSFET, uno en la superficie y otro en el cuerpo del transistor. Los electrones activados térmicamente son inyectados al contacto de compuerta a través de la región de traslape entre drenaje y compuerta, una situación que lleva al transistor a la condición de banda plana, bloqueando así el canal de conducción superficial y produciendo el efecto de resistencia negativa. Se propone entonces un modelo analítico que correlaciona bastante bien con los datos experimentales.

En el capítulo 2 pretendo proveer al lector de una perspectiva general de las diferentes metodologías que pueden llevar a la determinación de la corriente de cargas a través de un sistema nanométrico desde una perspectiva puramente de la mecánica cuántica. Comienzo con la información que, en principio, la mecánica cuántica no relativista puede proveer sobre cualquier sistema físico. Expongo las dificultades que surgen al querer aplicar la mecánica cuántica a la determinación de la corriente en un sistema nanométrico para posteriormente presentar una metodología más realista pero aún complicada representada por la mecánica estadística cuántica. Finalmente, se presenta una serie de suposiciones conocidas como el formalismo de Landauer, las cuales permiten la determinación de una expresión cerrada para la corriente en términos de la probabilidad de transmisión.

En el capítulo 3 se desarrolla una analogía entre las ecuaciones de Maxwell y Schrödinger independientes del tiempo aplicable a sistemas bidimensionales con

puertos de guía de onda. En los limites del sistema que colindan con las guías de onda, las condiciones de frontera de tercer orden para el campo eléctrico se reducen a la derivada normal de su componente en la dirección z, adoptando la misma forma de las condiciones de frontera equivalentes para la ecuación de Schrödinger. La energía total y la energía potencial dependiente de la posición son incluidas en el conjunto de cantidades que tienen un parámetro electromagnético equivalente. Los métodos electromagnéticos estándar fueron aplicados en la determinación de la función de onda y la probabilidad de transmisión de dispositivos electrónicos cuánticos coherentes incluyendo una estructura que permite tuneleo. La ecuación de Schrödinger fue resuelta con ayuda del "Quantum Transmitting Boundary Method" para una comparación directa con las simulaciones electromagnéticas.

Cuando se requiere de la caracterización y modelado del transporte de cargas en dispositivos semiconductores a escala nanométrica, el Formalismo de Funciones de Green Fuera de Equilibrio representa la metodología más prominente actualmente. De hecho, este formalismo puede ser considerado como el equivalente cuántico de la teoría de transporte de Boltzmann. En el capitulo 4 se presenta un análisis sistemático de varias nanoestructuras multipuerto bajo la influencia de un campo magnético., lo cuál representa una visión alternativa para la caracterización y modelado de dispositivos semiconductores a futuro.

To my mother,

the forgotten star I come from.

CONTENTS

CHAPTER 1:
Tunable Negative Differential Resistance Effect with a Single MOSFET

This chapter introduces an alternative way to produce a negative differential resistance (NDR) effect that is achieved by the non-conventional biasing of a regular 28-nm n-type Metal-Oxide-Semiconductor Field-Effect Transistor (n-MOSFET). It has a controllable peak-to-valley current ratio (PVCR) that goes from about 3.0 up to a room-temperature value of 5.5. Two bipolar mechanisms working in parallel are demonstrated to occur inside the n-MOSFET, one at the surface and other in the bulk. Thermally activated electrons are injected into the gate contact through the drain-gate overlap, a situation that leads the transistor to the flat-band condition, blocking the surface conduction channel and triggering the NDR effect. I proposed a simple analytical model that correlates very well with experimental data.

I. Negative Differential Resistance (NDR) Devices and Circuits

In this section a brief summary of the most relevant NDR devices and circuits, is introduced. For each case, the main differences with the proposed NDR effect are discussed.

A. NDR devices

Quantum tunneling devices. They work under quantum mechanical principles where a particle can tunnel through an energy potential barrier. The most prominent are the band-to-band tunneling (BBT) diode and the resonant tunneling (RT) diode [2,3]. A BBT diode consists of a p-n junction in which both regions are degenerately doped (>10^{19} cm^{-3}), see left column in Fig. **1**.**1**. Initially, a small forward bias voltage (V) produces a low current (I). This is because the high electron concentration

between E_C and $E_F(n^{++})$ in the n-type semiconductor is not aligned with the high concentration of empty states or holes between E_V and $E_F(p^{++})$ in the p-type semiconductor (top diagram). A larger V aligns these two regions of high concentration and if the depletion region is narrow enough (<10 nm), electrons can easily tunnel through, creating a current increment (middle diagram). A further increment of V produces a new misalignment between these two regions decreasing the current and producing the NDR effect (bottom diagram).

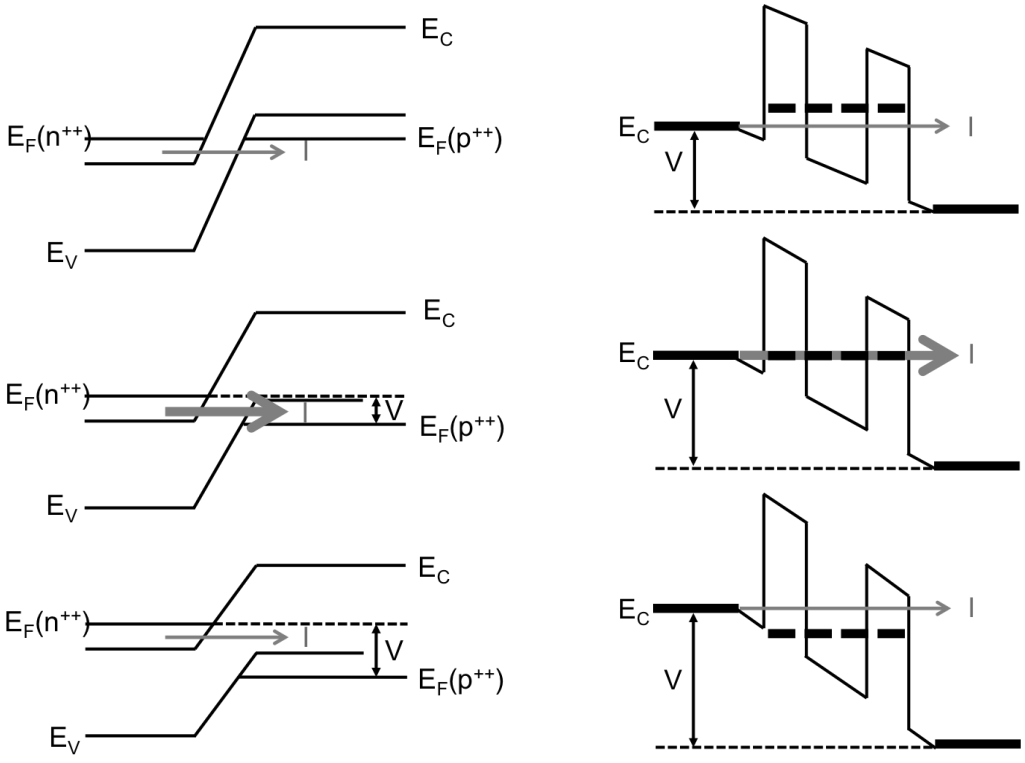

Fig. 1.1 Left column: Band-to-band tunneling operation. Right column: Resonant tunneling operation.

A RT diode is composed of two barrier layers (1.5-5 nm) enclosing a quantum well (~5 nm) that in turn are located in the middle of two highly doped contacts (see right column in Fig. **1**.**1**). The RT diode is similar to the BBT diode in that the high electron concentration sub-band above E_C, in the left contact, must be aligned with the high

transmission probability level (dashed thick line) originated by the resonant wave states between the two potential barriers. The BBT and RT mechanisms cannot be achieved with the 28-nm MOSFETs analyzed in this document since they do not match the required doping profiles. The maximum acceptor concentration in the bulk is $2 \cdot 10^{18}$.

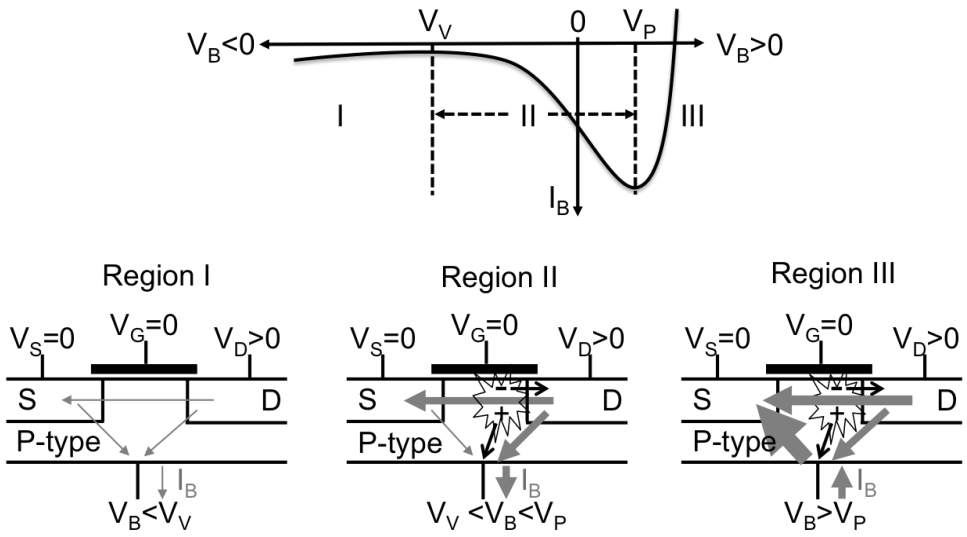

Fig. 1.2 Top: current diagram for the BGB device. Bottom: device diagram for each of the three operational regions.

Bistable Gated Bipolar (BGB) device or reverse base current in a bipolar transistor [4,5]. A BGB device exhibits a NDR effect at the bulk terminal (I_B) of a MOSFET structure biased in the sub-threshold regime (see Fig. **1.2**). The current voltage characteristics $I_B(V_B)$ is divided in three regions (I, II, and III) by the bulk voltages V_P and V_V corresponding to the peak and valley bulk currents $I_B(V_B = V_P)$ and $I_B(V_B = V_V)$, respectively. In Region I, I_B is negative and low in magnitude because the drain- and source-bulk junctions are backward-biased. The sweep of V_B towards positive values causes, in region II, a reduction of the threshold voltage V_{th}, which in turn raises the surface current. This increment stimulates impact ionization at the drain depletion region, raising I_B negatively and triggering the NDR phenomenon. In Region III, the source-bulk junction is forward-biased, increasing the

bulk-to-source current exponentially; a situation that eventually inverts I_B. The NDR effect of our n-MOSFETs is observed at the drain and source terminals, not at the bulk terminal. Besides, the drain-bulk junction is forward-biased below the high-impact ionization regime in our case.

Negative transconductance in double-gate FETs [6]. The authors attribute the observed negative subthreshold front gate transconductance g_{FG} and back gate transconductance g_{BG} to the charge coupling between the two inversion channels in a double-gate FET. When the front gate voltage raises, the carrier density in the front and back channels increase. As a result, the total current increases initially. However, due to a step-like mobility which drops substantially for increments of the charge density, the total current drops too, causing the negative transconductance effect (see Fig. **1.3**). There is no evidence to believe that the n-MOSFETs of this document have a step-like mobility.

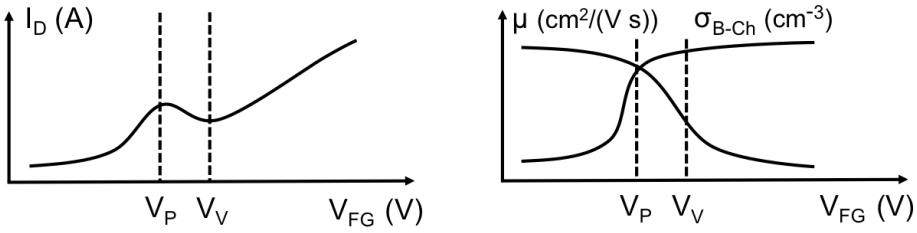

Fig. 1.3 Left: front-gate voltage (V_{FG}) vs. drain current (I_D). Right: step-like mobility μ and back-channel electron density σ_{B-Ch} against V_{FG}.

NDR in SOI-MOSFETs [7]. This NDR effect has been observed for both p- and n-channel SOI-MOSFETs, with short and long channels, and is attributed to a mobility reduction caused by local heating in the channel region. In this sense, this effect is similar to the previous case, but this time, the mobility reduction results from relatively poor thermal properties of the buried insulators compared with silicon bulk substrates. This behavior has been also observed in power devices. On the other hand, the n-MOSFETs I worked with do not have any kind of isolation between the bulk contact and the channel region.

Bulk NDR devices [8]. Bulk-effect semiconductor devices are structures only composed of a bulk semiconductor with ohmic contacts (e.g. no p-n junctions). They show interesting phenomena working under various external influences such as electric and magnetic fields. The bulk NDR devices can be classified into two groups: voltage-controlled and current-controlled (see Fig. **1.4**). For this devices, the negative resistivity is associated with microscopic bulk semiconductor properties, such as 1) field enhanced trapping, 2) impact ionization of shallow impurity levels in compensated semiconductors, or 3) electron transfer from a lower valley to higher valleys in the conduction band.

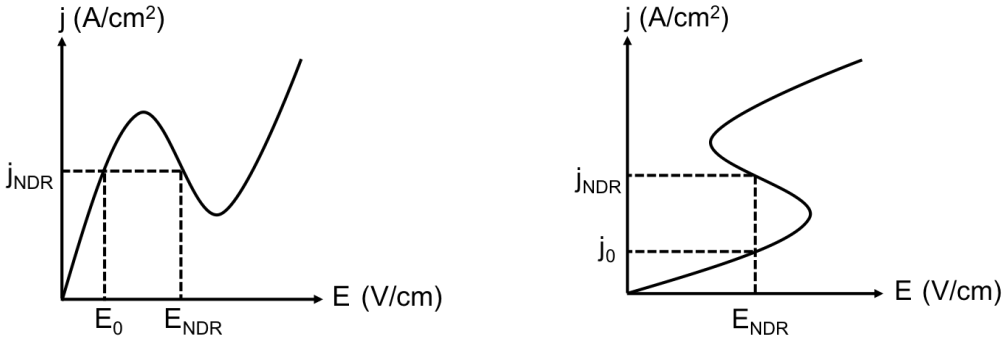

Bulk voltage-controlled NDR Bulk current-controlled NDR

Fig. 1.4 Bulk voltage- and current-controlled negative differential resistivity.

The Cryosar is a bulk current-controlled NDR device. It has the potential to be used in high-speed switching and memory applications. At low temperatures (e.g., liquid helium temperature of 4.2 K) with low applied voltages, the bulk semiconductor may have a very high resistivity, since almost all the carriers are attached to the impurity centers. As the applied voltage increases, it becomes possible for the free carriers to gain sufficient energy in the electric field to ionize the impurities upon impact. At some critical electric field, the impact ionization rate exceeds the recombination rate and when almost all the impurities are ionized the resistivity reduces by many orders of magnitude. Therefore, the right plot in Fig. **1.4** shows that for the same magnitude of the electric field E_{NDR}, there can be two different values

for the current density: a lower current j_0 for a large resistivity stage prior to impact ionization and a higher current j_{NDR} for the low resistivity stage afterwards. On the other hand, the NDR effect introduced in this document can be observed at room temperature and, as stated before, do not occur under the high-impact ionization regime.

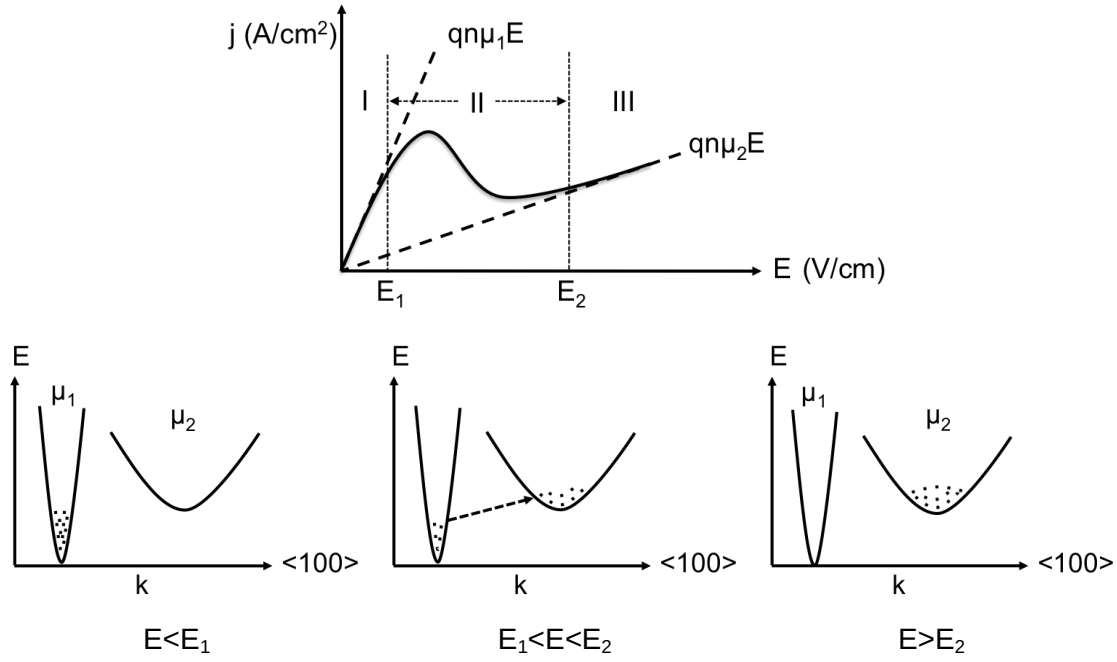

Fig. 1.5 Top: j-V characteristics of a transferred-electron NDR device. Bottom: Electron distributions under various conditions of electric fields.

The transferred-electron or Gunn effect [8] is a bulk voltage-controlled NDR effect that occurs in n-type GaAs and, under uniaxial pressure, in InP, CdTe, ZnSe, and InAs. In this materials conduction-band electrons can be field-induced transferred from a low-energy high-mobility valley to higher-energy low-mobility satellite valleys as shown in Fig. **1.5**. It can be seen that in Region I (low applied voltages), electrons travel mainly through high-mobility μ_1 current carrying states. In Region III (high applied voltages), electros travel mainly through low-mobility $\mu_2 < \mu_1$ current carrying states. The NDR effect can be observed in Region II as a transition

from Region I to Region III. However, the NDR effect studied in the next section is observed in silicon MOSFETs that are composed of different p-n junctions.

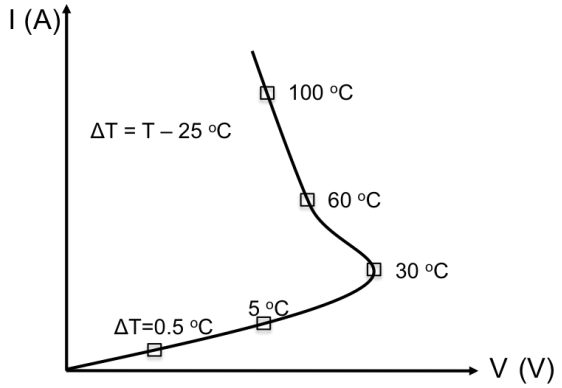

Fig. 1.6 I-V characteristics of a thermistor.

A thermistor or thermally sensitive resistor is a bulk current-control NDR device that has an ohmic behavior for small currents. However, as the current increases, the power dissipation also increases and the resistivity of the material $\left[q\left(n\mu_n + p\mu_p\right)\right]^{-1}$ decreases because the majority carrier concentration in a semiconductor varies approximately as exp(-A/T) where T is the temperature and A is a constant depending on the band gap and impurity concentrations (see Fig. **1**.**6**). The mobility of the majority carriers reduces at a lower rate compared to the majority carrier concentration.

Dynatron [9]. This is an active two-port vacuum device that reproduces a NDR effect operating under impact ionization (see the circuit diagram and the I-V characteristics in Fig. **1**.**7**). Initially, electrons are set in motion by the electric field between the filament and the anode. Some of them go thru the anode holes and reach the plate, which is at a low potential with respect to the filament. Although catching some electrons, the plate is actually repelling them due to its lower potential. The number of “arriving” electrons depends on the filament temperature and is practically independent of the voltage of the plate. These arriving electrons generate a current in the external circuit. Besides, if the potential of the plate is raised, the velocity with which the electrons strike it will increase, generating electrons that leave the plate by impact ionization. These “leaving” electrons will be

collected by the more positive anode contact generating a current in the opposite direction and setting up two competing mechanism. Since the number of leaving electrons increases rapidly with the increments of the voltage plate, the total current starts to decrease at point A. When the number of arriving and leaving electrons is the same, the total current is zero (point B). Eventually, the total current inverts when the number of leaving electrons is larger than the number of arriving electrons (point C). Ultimately, the total current again inverts at point D when the plate reaches the anode potential. At this point, the anode does not collect the leaving electrons anymore; the plate recollects them.

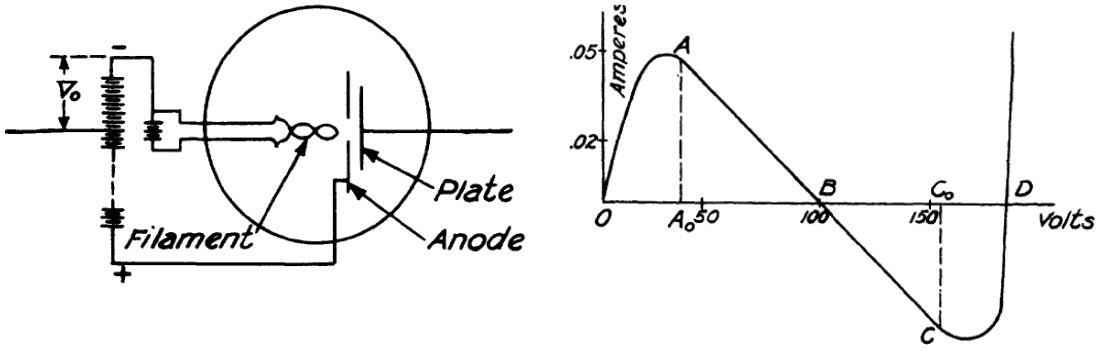

Fig. 1.7 Left: Dynatron circuit diagram. Right: total current vs. plate voltage [9].

B. NDR circuits

Cross-Coupled Feedback Structure (CCFS) [10]. The authors of this work (Leon O. Chua et al.) stated that hundreds of NDR circuits, made of two transistors and linear positive resistors only, can be generated by using a systematic method. The two transistors may be bipolar (n-p-n or p-n-p), JFET (n-channel or p-channel), MOSFET (n-channel or p-channel), or their combinations. The authors to not provide a demonstration but instead they present an algorithm that render candidates for voltage-controlled and current-controlled NDR circuits (i.e. not all candidates will exhibit a NDR characteristic). The following three-step algorithm is for voltage-controlled NDR circuits (I refer the reader to the source for the equivalent current-

controlled NDR algorithm). 1) Start with the two-transistor feedback structure shown in Fig. **1**.**8**, where T_1 and T_2 represent any pair of transistors from the list just mentioned. The starred terminals represent ether the gate or base of the chosen transistors. 2) Connect a source current across any pair of nodes of the resulting feedback circuit. 3) Connect any number of linear positive resistors across any pair of nodes or across two points of the same branch. It is not needed to connect a resistor in series or in parallel with the current source. Finally, there is only need to verity if the resulting circuit exhibits a NDR effect. An example of a cross couple feedback structure is the Ultra-Low Power (ULP) diode [11]. On the other hand, the two BJT mechanisms within a single MOSFET that will be discussed later in this document are not interconnected in a cross-coupled feedback structure but in parallel.

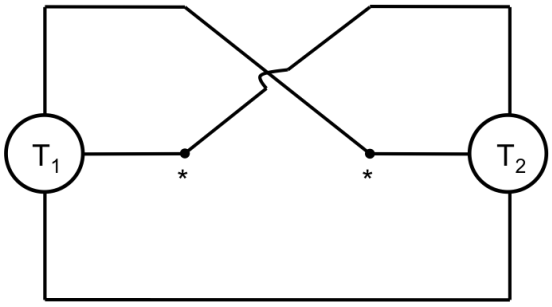

Fig. 1.8 Two-transistor ¨cross-cooupled¨ feedback structure.

Polysilicon Gated-Nano-Wires (polySiNW) [12]. A hybrid NDR circuit made by a particular connection of one n-MOSFET and one polySiNW that uses positive feedback has been reported. When operated at constant current, the polySiNW transfers its negative slope output characteristic (see Fig. **1**.**9**a) to the I-V characteristics of the MOS transistor that is driving a much higher output current to produce the NDR effect (see Fig. **1**.**9**b). In our proposal, the gate potential drop is not assisted by an external device, but it is self-induced as will be shown later.

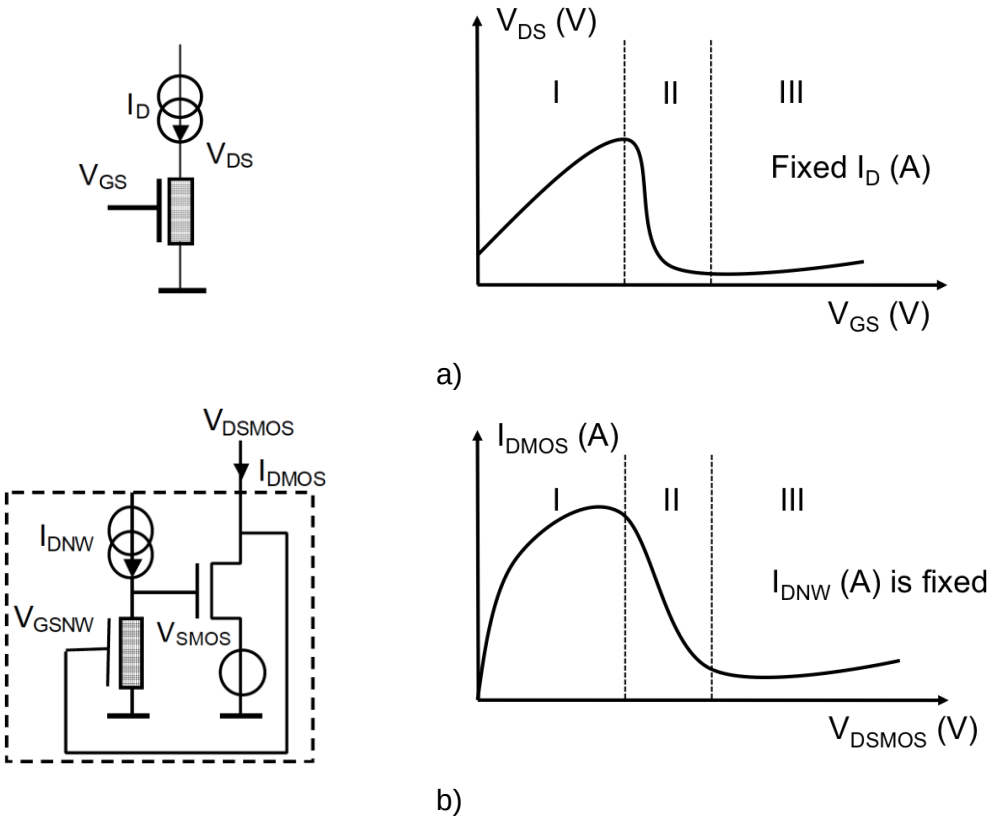

Fig. 1.9 a) Diagram of the polysilicon Gated-Nano-Wire (polySiNW) in series with a constant current source I_D and the V_{DS}-V_{GS} characteristics. b) Diagram and resulting I_{DMOS}-V_{DMOS} characteristics of the NDR circuit composed of the polySiNW and a MOS transistor.

Series-Connected NDR Devices [13]. Numerous circuits using two or more NDR devices in the series integration can be applied to create a multiple-peak curve in the combined I-V characteristics.

II. Analysis and Characterization

This work proposes a novel CMOS-compatible NDR structure. This device does not use any of the principles of operation of the NDR devices and circuits mentioned before, but two self-contained bipolar junction mechanisms working in parallel within a single floating-gate MOSFET.

The devices used in the experiments are n-MOSFETs of a 28-nm CMOS technology fabricated with Hafnium Oxide (HfO_2) dielectrics and metallic gates. These devices have a H_fO_2 thickness of 4 nm, a 1.5-nm thick interfacial layer, a channel width W of 1 µm, and channel lengths L of 34, 38, 42, 60 and 500 nm. Fig. **1**.**10** depicts the negative resistance effect for these transistors. The key fact is to leave the gate floating ($I_G = 0.0\ A$) while the drain voltage V_D is swept from zero to negative values. In this case the source voltage V_S and the bulk voltage V_B are grounded. Note that the 34-nm transistor is the one that has the largest peak-to-valley current ratio (PVCR) and the 500-nm transistor has the smallest one. Herein, an explanation of the mechanisms behind the three regions marked in Fig. **1**.**10** is introduced.

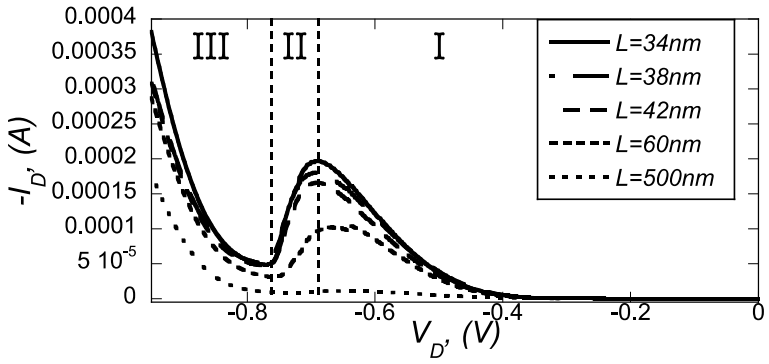

Fig. 1.10 Measured I_D-V_D characteristics with the gate contact floating, $V_S = 0.0\ V$ and $V_B = 0.0\ V$. (W/L)=(1 µm/34, 38, 42, 60, 500 nm) n-MOSFETs at T=300 K.

In general, any charge accumulation near the transistor channel leads to threshold voltage shifts [14]. When the density of trapped charge changes during a measurement, a hysteresis effect is visible. Moreover, if enough charge gets trapped in a short period of time, it is possible to observe a NDR effect. For example, an

abrupt current decrease in a nanowire has been reported to occur when a floating quantum point is charged with the help of a control gate similarly to a flash memory [15]. The remarkable difference is the number of trapped electrons needed to block the conduction channel.

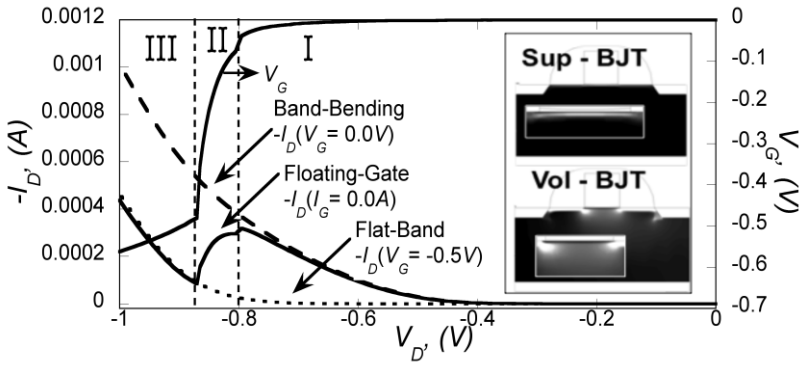

Fig. 1.11 Continuous I_D curve, floating-gate condition; dotted and dashed curves, flat-band condition ($V_G = -0.5$ V) and band bending condition ($V_G = 0.0$ V), respectively. In all cases $V_S = 0.0$ V and $V_B = 0.0$ V. (W/L)=(1 µm/60 nm) n-MOSFET at T=300 K. The inset shows simulations of the electron current density inside a 60-nm n-MOSFET under band bending conditions in region I (Sup-BJT) and under flat band conditions in region III (Vol-BJT).

The present approach consists in treating the drain, source and bulk contacts of an n-MOSFET as the emitter, collector and base of a Bipolar Junction Transistor (BJT), respectively. The dashed curve in Fig. **1.11** shows the measured I_D when V_D is swept from zero to negative values with all the other terminals grounded. In this case, current starts to flow at the surface (region I) and later in the bulk (region III) since the potential barrier is lower at the substrate-oxide interface due to undesired trapped charges and the built-in potential between gate and bulk. The dotted curve was measured under flat-band conditions so that only the volumetric current flows (region III). Two BJT mechanisms working in parallel can be identified, one at the surface (sup-BJT) and other in the bulk (vol-BJT). The inset illustrates the simulated current density that corresponds to these two mechanisms. Therefore, when the gate is floating (continuous I_D curve), the transistor switches from the sup-BJT (region I) to the vol-BJT (region III) triggering the NDR effect (region II). The measured gate

voltage (V_G) reflects theses facts. In region I, the bands remain bent ($V_G = 0.0\ V$), while in region II, V_G drops abruptly, indicating a surface-band straightening process which continue until the flat-band condition is reached.

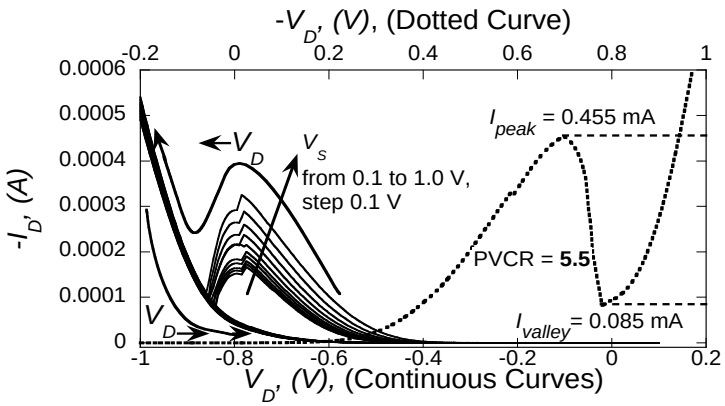

Fig. 1.12 Continuous curves: Measured I_D-V_D with V_S as a parameter. V_D is swept in two directions, from 0.0 to -1.0 V and from -1.0 to 0.0 V. $V_B = 0.0\ V$ and the gate is floating. (W/L)=(1 µm/60 nm) n-MOSFET at T=300 K. Dotted curve: Measured I_D - V_D characteristics with $V_S = 1.0\ V$, $V_B = 0.0\ V$, and the gate floating. (W/L)=(1 µm/34 nm) n-MOSFET at T=300K.

As shown in Fig. **1.12**, V_S controls the PVCR. The higher the source voltage is, the larger the drain current is, in agreement with the bipolar mechanism hypothesis. Fig. **1.12** also shows a hysteresis effect. If V_D is swept from 0.0 V to -1.0 V the sup-BJT turns on, otherwise it does not. The dashed curve, which corresponds to a 34-nm n-MOSFET, presents the maximum PVCR=5.5 measured at room temperature.

III. Qualitative and Quantitative Modeling

I begin the explanation by assuming that the system has reached equilibrium before carrying out the measurements. This means that if all contacts are grounded, the floating gate voltage must be also zero after some time. To accelerate the relaxing

process, the gate can be grounded and disconnected to release it from any charge excess.

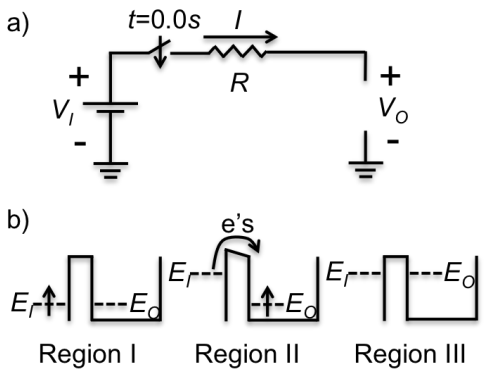

Fig. 1.13 a) Circuit diagram of a floating port $\mathrm{V_O}$. b) Band diagrams of the floating port with quasi-Fermi level $\mathrm{E_O}$ separated by a potential barrier from the input port with quasi-Fermi level $\mathrm{E_I}$ for each of the three operational regions.

Fig. **1**.**13a** shows the circuit representation of a floating port with voltage $\mathrm{V_O}$. When the switch is closed at $\mathrm{t = 0.0\ s}$, charges start to flow across the resistance and start to build up on the other side, reducing the electric field inside the circuit to its minimum value according to Gauss law. This happens almost instantaneously and very quickly $\mathrm{V_I = V_O}$. In contrast, the charging process is much slower if a potential barrier separates the input reservoir from the floating port, both with quasi-Fermi levels $\mathrm{E_I}$ and $\mathrm{E_O}$, respectively (see Fig. **1**.**13b**). Initially, when $\mathrm{E_I}$ starts to be raised as a result of a negative potential applied to that contact, very few electrons can be thermally activated to get over the barrier. As a consequence, $\mathrm{E_I}$ remains unchanged and a potential drop between input and floating port is established. This situation corresponds to region I in Fig. **1**.**11**. As $\mathrm{E_I}$ is further raised, electrons gain enough energy to surpass the barrier at a larger rate and the charging process of the floating port is now evident, which corresponds to region II. This happens until $\mathrm{E_I = E_O}$, a moment when the floating port is considered to be full (region III).

This qualitative model describes very well the measurements of $\mathrm{V_S}$ when the source is floating, $\mathrm{V_G}$ is used as a parameter, $\mathrm{V_D}$ is swept from 0 to -1 V, and $\mathrm{V_B = 0.0\ V}$ (see Fig. **1**.**14**). Decrements of $\mathrm{V_G}$ increase the potential barrier height at

the substrate surface between drain and source, shifting the onset of regions II and III towards negative V_D values. Notice that $V_S = V_D$ in region III as predicted. This figure also shows the measured V_G of Fig. **1.11**. The main difference with the previous case is that $V_G \neq V_D$ in region III. This is attributed to the V_G-dependent leakage current through the oxide between gate and substrate that acts as a voltage divider. Electron thermal emission from drain to gate is possible due to the relatively small potential barrier between Si and HfO2 whose height was reported to be 1.13 ± 0.13 eV [16]. A barrier height of 0.95 eV was experimentally obtained from a Richardson plot (inset of Fig. **1.15**). This model also explains the hysteresis effect of Fig. **1.12** since reversing the direction of V_D, leaves the gate charged.

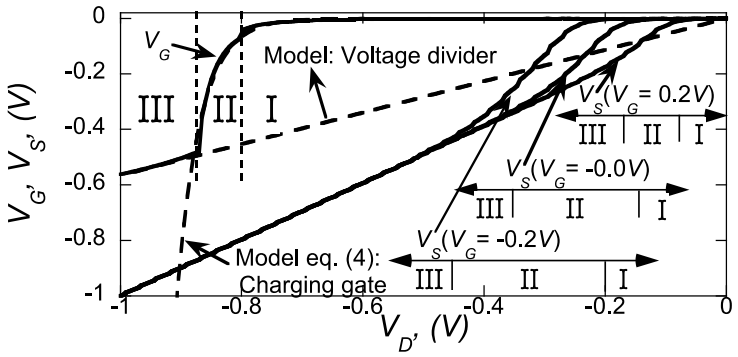

Fig. 1.14 Measured V_S-V_D for different V_G values and $V_B = 0.0\,V$. Comparison between the measured V_G of Fig. **1.11** and the proposed model for regions I-II and for region III.

The floating gate voltage V_G is determined from its quasi-Fermi level E_F, which in turn is related to the charge concentration in this contact. Due to its large dimensions, a three-dimensional density of states can be assumed. The corresponding expression is

$$E_F = \frac{\hbar^2}{2m^*}\left[\frac{3\pi^2 N}{V}\right]^{2/3}, \qquad (1.1)$$

where m^* is the effective mass, $\hbar$ is the Plank constant, V is the volume, and $N = \frac{1}{q}\int_0^t I dt$ is the number of injected electrons provided by the drain across the gate-drain overlap. The electron charge is q and the gate-drain current I is approximated by the Schottky junction expression

$$I = I_0\left(e^{\frac{-V_d(t)}{nV_t}} - 1\right) \; I \approx I_0 e^{\frac{-V_d(t)}{nV_t}}, \tag{1.2}$$

such that I_0 is the saturation current, n the ideality factor, and V_t the thermal voltage. The drain voltage is a ramp ($V_d(t) = -Bt$). Therefore, the expression for the number of injected charges is

$$N = \frac{I_0 n V_t}{qB}\left(e^{\frac{-V_d(t)}{nV_t}} - 1 + \frac{V_d(t)}{nV_t}\right). \tag{1.3}$$

Neglecting the non-exponential terms inside the parenthesis of equation (**1.3**), substituting the result in (**1.1**) and dividing by the electron charge, the final expression for the gate voltage in region II is

$$V_G \approx -\frac{\hbar^2}{2m^* q^{\frac{5}{3}}}\left(\frac{3\pi^2 I_0 n V_t}{BV}\right)^{\frac{2}{3}} e^{-\frac{2V_d(t)}{3nV_t}}. \tag{1.4}$$

Since the experiments were performed under quasi-DC conditions, the non-zero total current, $I = I_D + I_S + I_B$, can be attributed entirely to the charging process (see Fig. **1.15**). By fitting the Schottky expression (**1.2**) to the experimental total current I, the parameters n and I_0 were determined. In these measurements $B = 300\ mV/s$ and for the current analysis $V_t = 0.026\ V$. The aluminium interconnection pad is the biggest segment of the gate electrode, then $V \approx 100 * 100 * 1\ \mu m^3$ and $m^* = 1.1\ m_{free}$. Finally, Fig. **1.14** and Fig. **1.15** show the good correlation between the measured Vg and the model of eq. (**1.4**), within region I, and region II.

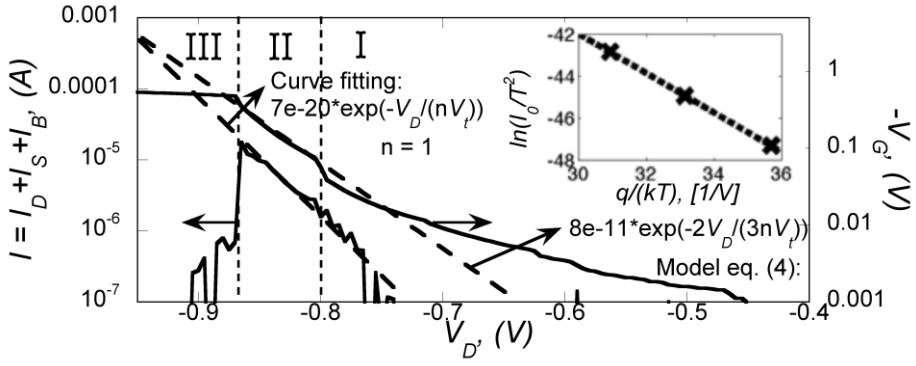

Fig. 1.15 Total current (I) and gate voltage with their corresponding curve fitting and model, respectively. The inset shows the Richardson plot with data at T = 325, 350 and 375 K.

IV. Conclusions

Two BJT mechanisms where demonstrated to occur in a single n-MOSFET. By non-conventionally biasing the n-MOSFETs, the floating gate gets charged, turning off the superficial conduction channel and triggering the NDR effect. In a way that resembles a flash memory, the drain itself works as the control gate, and the main charging mechanism is not quantum tunneling but thermal emission. A simple analytical model for the floating ports that correlates very well with experimental data was implemented.

CHAPTER 2:
Quantum Transport: Landauer Formalism

This chapter provides a general perspective of the theoretical approaches that can lead to the determination of the charge current through a nano-scaled system from a full quantum mechanical perspective. It exposes the amount of information that, in principle, can be obtained from any physical system and the complications that arise in the determination of the current. The more realistic but still very difficult statistical quantum mechanical approach is briefly presented afterwards. Finally, the Landauer formalism is established as a series of assumptions that render a close-form expression for the current in terms of the probability of transmission.

I. Quantum Mechanics: General Case

The five postulates, axioms or principles of quantum mechanics are the basic rules in the determination of the dynamics of any physical system. By basic rules I mean the mathematical background and the connection between theory and experiment. In other words, these postulates answer the following questions: 1) How is the state of a quantum system at a given time described mathematically? 2) Given this state, how is it possible to predict the results of the measurement of different physical quantities? 3) How can the state of the system at time t be found when the state at time t_0 is known?

A. Postulate 1: System State

The state of any physical system is completely determined at time t_0 by a state vector, $|\Psi(t_0)\rangle$, that belongs to a Hilbert space (i.e. a vector space with an inner product).

B. Postulate 2: Observables

To every physically measurable quantity A called dynamical variable or observable, it can be assigned a linear Hermitian operator $\hat{A}$ whose eigenvectors form a complete basis of the Hilbert space that contains $|\Psi(t)\rangle$. This operator has, in general, a spectrum of eigensolutions with discrete components,

$$\hat{A}|\Psi_n\rangle = a_n|\Psi_n\rangle\,, \tag{2.1}$$

but mainly a continuum spectrum,

$$\hat{A}|\Psi_a\rangle = a|\Psi_a\rangle\,. \tag{2.2}$$

The result of a measurement is either a discrete eigenvalue a_n or a value in the interval of continuous eigenvalues $(a, a + \Delta a)$ depending on the equipment resolution Δa. Therefore, the state of the system can be written as a linear superposition of the eigenvectors, discrete and continuous, of the operator $\hat{A}$:

$$|\Psi(t)\rangle = \sum_n c_n(t)|\Psi_n\rangle + \int c_a(t)|\Psi_a\rangle da, \tag{2.3}$$

where the coefficients $c_n(t)$ and $c_a(t)$ are complex numbers.

C. Postulate 3: Measurements

A measurement of the quantity A may be represented by the application of the operator $\hat{A}$ on the state vector $|\Psi(t)\rangle$. If the state of the system is given by (**2.3**) before the measurement of A, and a discrete eigenvalue a_n is observed by measuring it at time t, the system is in the state

$$|\Psi(t+dt)\rangle = |\Psi_n\rangle, \tag{2.4}$$

immediately after the measurement. For a measurement in the continuum instead, if a value in the interval $(a, a+\Delta a)$ is measured, the system is in the state

$$|\Psi(t+dt)\rangle = \left(\int_a^{a+\Delta a} |c_a(t)|^2 da\right)^{-1/2} \int_a^{a+\Delta a} c_a(t)|\Psi_a\rangle da, \tag{2.5}$$

where again, Δa is the precision of the measuring apparatus.

D. Postulate 4: Probabilistic outcome of Measurements

Discrete spectra

If the state vector is normalized (i.e. $\langle\Psi(t)|\Psi(t)\rangle = 1$), the probability of obtaining one of the non-degenerated eigenvalues a_n of the corresponding operator $\hat{A}$ when measuring an observable A of a system in a state $|\Psi\rangle$ is:

$$P_n(t) = |\langle\Psi_n|\Psi(t)\rangle|^2 = |c_n(t)|^2 . \tag{2.6}$$

If the eigenvalue a_n is m-degenerate, the probability becomes

$$P_n(t) = \sum_{j=1}^{m} \left|\langle\Psi_n^j|\Psi(t)\rangle\right|^2 = \sum_{j=1}^{m} \left|c_n^j(t)\right|^2. \tag{2.7}$$

Continuous non-degenerate spectra

The probability density that a measurement of $\hat{A}$ yields a value between a and $a+da$ on a system which is initially in state $|\Psi\rangle$ is

$$\frac{dP_a(t)}{da} = |\langle\Psi_a|\Psi(t)\rangle|^2 = |c_a(t)|^2. \tag{2.8}$$

E. Postulate 5: Time evolution

The time evolution of the state vector $\Psi(t)$ of a system is determined by the Schrödinger equation

$$i\hbar\frac{d}{dt}|\Psi(t)\rangle = \hat{H}(t)|\Psi(t)\rangle\,, \tag{2.9}$$

where $\hat{H}(t)$ is the Hamiltonian operator corresponding to the total energy of the system. In general, $\hat{H}$ is the many-body Hamiltonian, sum of the kinetic energy of all particles, all interaction energies between them, and any other interaction energy (e.g. the one due to external fields). There is no indeterminacy in the time evolution of a quantum system. Indeterminacy appears only when a physical quantity is measured. However, between two measurements, the state vector evolves in a perfectly deterministic way, in accordance with equation (**2**.**9**).

II. Quantum Mechanics: Carrier transport

Since in this work the interest is focused on the quantum transport of charge carriers through nanostructures, the corresponding Hamiltonian $\hat{H}$ and current operator $\hat{I}$ must be specified. The former represents the system under study and the later the measuring apparatus. As stated, the act of measuring is the application of the operator $\hat{I}$ on the state vector $|\Psi(t)\rangle$, which is a solution of the Schrödinger equation. Then, for a system under the influence of a time-dependent electromagnetic field, the current density operator can be stated as

$$\hat{\mathbf{j}}(\mathbf{r}, t_0) = \frac{1}{2}\sum_i \{\delta(\mathbf{r} - \hat{\mathbf{r}}_i), \hat{\mathbf{v}}_i\}, \tag{2.10}$$

where the sum extends to all particles with position operator $\hat{\mathbf{r}}_i$ and velocity operator $\hat{\mathbf{v}}_i = (\hat{\mathbf{p}}_i - e\mathbf{A}(\mathbf{r}, t)/c)/m$. Here, $\hat{\mathbf{p}}_i$ is the momentum operator, $\mathbf{A}(\mathbf{r}, t)$ is the vector potential, e is the electron charge and m its mass. Besides, for any two operators $\hat{B}$

and $\hat{C}$, the anticommutation relation is defined by $\{\hat{B},\hat{C}\} = (\hat{B}\hat{C} + \hat{C}\hat{B})$. Integrating the current density operator over a surface S, the current operator can be determined,

$$\hat{I} = \int d\mathbf{S} \cdot \mathbf{j}(\mathbf{r}, t). \tag{2.11}$$

Since a measurement provides, at most, a probabilistic outcome, it is of practical interest to calculate the average or expectation value among all possible outcomes or results of measuring $\hat{I}$ when the system state is $|\Psi(t)\rangle$. In formal terms, the expectation value of an observable can be determined as follows: prepare a very large number of identical systems each in the same state $|\Psi(t)\rangle$. The observable $\hat{I}$ is then measured on each of these identical systems. Then, the average value of all these repeated measurements is called the expectation value of $\hat{I}$ with respect to the normalized state $|\Psi(t)\rangle$ and can be expressed as:

$$I = \langle \hat{I} \rangle = \langle \Psi(t) | \hat{I} | \Psi(t) \rangle. \tag{2.12}$$

III. Statistical Quantum Mechanics

Modeling a transistor-like device (i.e. considering the conduction channel and contacts) using the Schrödinger equation is extremely difficult, since it is composed of millions of atoms (e.g. the density of atoms of a silicon crystal is about 5 x 10^{10} atoms/um^3). The state vector $|\Psi(t)\rangle$ of such a system would have 3N degrees of freedom, where N is the number of particles that compose the system. The needed initial condition $|\Psi(t_0)\rangle$ to solve the Schrödinger equation at time t cannot be provided by an average quantity like a current measurement. To determine the state vector at a specific moment t_0 means that the maximum amount of information has to be known at that instant, according to the uncertainty principle. This means that in order to find $|\Psi(t_0)\rangle$, a complete set of commuting observables has to be measured. In simple words, a series of measurements must be performed before $|\Psi(t_0)\rangle$ is determined and each measurement must be independent of the others. For example position and momentum observables do not commute since a measurement of one

disturbs the other. It is clear that if a quantum mechanical approach to the carrier transport in nanostructures is desired, a set of simplifications is needed.

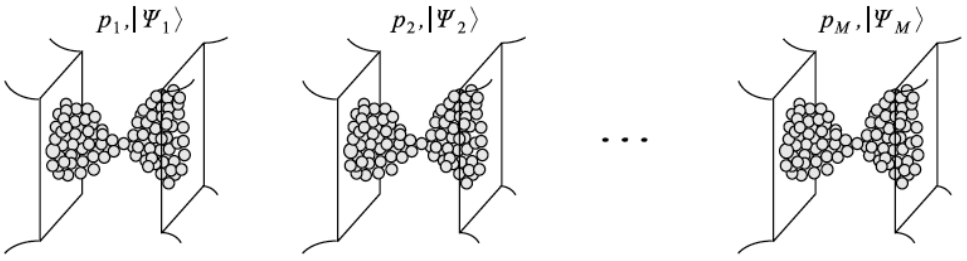

Fig. 2.1 An ensemble of identical copies of a system, each described by a state vector $|\Psi_i(t)\rangle$ occurring with probability p_i.

A. Statistical Quantum Mechanics: Closed Systems

If the quantum-mechanical state of the system is not known exactly, it can only be discussed what is the probability p_i that the system is in the state $|\Psi_i(t)\rangle$ at any given time t. It is thus convenient to envision an ensemble of identical copies of the system, all prepared with similar, but not necessarily identical, initial conditions (see Fig. **2**.**1**). Then, the set $\{p_i, |\Psi_i(t)\rangle\}$ of all possible micro-states $|\Psi_i(t)\rangle$ and their probability p_i of occurring in the ensemble is called a macro-state of the system, or a mixed state. In order to represent a probability, the classical probabilities $\{p_i\}$ have to add to unity ($\sum_i p_i = 1$).

The density operator or statistical operator is a useful way to describe a quantum system in a mixed state (i.e. a statistical ensemble of several quantum states). By definition the density operator is

$$\hat{\rho}(t) = \sum_i p_i |\Psi_i(t)\rangle\langle\Psi_i(t)| \,. \tag{2.13}$$

The equation of motion for the density operator known as the Liouville−von Neumann equation can be easily obtained from the time-dependent Schrödinger equation (**2**.**9**) and turns out to be

$$i\hbar \frac{d\hat{\rho}(t)}{dt} = \left[\hat{H}, \hat{\rho}(t)\right], \tag{2.14}$$

where $\left[\hat{B}, \hat{C}\right] = \left(\hat{B}\hat{C} - \hat{C}\hat{B}\right)$ is the commutator of any two operators $\hat{B}$ and $\hat{C}$. By performing both a quantum-mechanical average over the normalized states of the system, and a classical average over the ensemble, the expectation value of the current operator is

$$\langle \hat{I} \rangle = \sum_i p_i \langle \Psi(t)_i | \hat{I} | \Psi(t)_i \rangle = \mathrm{Tr}(\hat{\rho}(t)\hat{I}). \tag{2.15}$$

The above results can also be extended to the case in which the Hamiltonian itself is not known exactly (i.e., when the Hamiltonian $\hat{H}$ contains some unknown components, or components that may vary randomly). Let us call $\hat{H}_j$ each Hamiltonian in this ensemble of random or stochastic Hamiltonians, and $\tilde{p}_j$ the probability that this Hamiltonian appears in the ensemble. Then, it can be defined a density operator

$$\hat{\rho}(t) = \sum_j \tilde{p}_j \hat{\rho}_j(t)\,, \tag{2.16}$$

where each $\hat{\rho}_j(t)$ is of the kind of equation (**2**.**13**) that satisfies expression (**2**.**14**) for a given Hamiltonian $\hat{H}_j$. The time evolution of $\hat{\rho}(t)$ is not known in a closed form, and in order to find it, one needs to evaluate the average (**2**.**16**), at every time step, over all stochastic evolutions of each element of the ensemble of Hamiltonians. Despite of it, the expectation value can be expressed as

$$\langle \hat{I} \rangle = \sum_j \tilde{p}_j \mathrm{Tr}\left(\hat{\rho}_j(t)\hat{I}\right). \tag{2.17}$$

B. Statistical Quantum Mechanics: Open Systems

Consider now the case in which the system can be separated into two subsystems, the nano-system under study and everything external to it (e.g. the measuring equipment or battery). In this case, it would be necessary to solve for the total Hamiltonian $\hat{H}_{Tot}$ that describes de dynamics of the particles (e.g. electrons and ions) conforming the nano-system of interest ($\hat{H}_S$), plus those particles corresponding to the external circuit ($\hat{H}_E$), and the interactions between these two systems $\hat{H}_{S-E}$,

$$\hat{H}_{Tot} = \hat{H}_S \otimes \hat{1}_E + \hat{1}_S \otimes \hat{H}_E + \hat{H}_{S-E}, \tag{2.18}$$

where $\hat{1}_S$ and $\hat{1}_E$ are the identity operators in the Hilbert space of the nano-system and the external circuit, respectively. The tensor product is represented by the symbol $\otimes$.

If the interest is focused in the dynamics of the electrons alone in the nano-system, the density operator can be calculated by tracing out all degrees of freedom associated with the external circuit from the statistical operator $\hat{\rho}_{Tot}(t)$ of the total system (i.e. one of the type of (**2.13**)), and maintaining only the degrees of freedom associated with the nanoscale system

$$\hat{\rho}_S(t) = Tr_E\{\hat{\rho}_{Tot}(t)\}. \tag{2.19}$$

In general, this does not lead to a closed equation of motion for the reduced statistical operator $\hat{\rho}_S(t)$. Nonetheless, if it is assumed that the battery degrees of freedom are dense in energy, and all their correlation times are very short compared to the electron dynamics –namely, the degrees of freedom of the battery are much faster than the degrees of freedom of the system– an equation of motion of the form known as Linbland or master equation can be written as

$$\frac{d\hat{\rho}_S(t)}{dt} = \mathcal{L}\hat{\rho}_S(t), \tag{2.20}$$

for some super-operator $\mathcal{L}$. The expectation value in this case is

$$\langle \hat{I} \rangle = \mathrm{Tr}(\hat{\rho}_S(t)\hat{I}). \tag{2.21}$$

IV. Landauer Formalism

The Landauer formalism consists of a series of simplifications that lead to a closed-form expression of the current. I will expose these approximations in the rest of this chapter starting from the assumption of having an open nano-scaled system (one exposed to external contacts) whose dynamics can be described by an equation of the type (**2.20**).

A. Approximation I: Ideal Steady State

For an arbitrary operator $\mathcal{L}$, equation (**2.20**) may or may not have a steady state solution in the long-time limit. In other words, a density operator $\hat{\rho}_S$ such that $\lim_{t\to\infty} d\hat{\rho}_S(t)/dt = 0$ may or may not exist. If it does, this solution may not be unique. To assume that (**2.20**) does admit a unique stationary solution is the first simplification in the Landauer formalism. Then, the expectation value simplifies to:

$$\langle \hat{I} \rangle = \mathrm{Tr}\left(\hat{\rho}_S \hat{I}\right) = \mathrm{constant}. \tag{2.22}$$

B. Approximation II: Mean-Field Approximation

An arbitrary partitioning of the system's Hamiltonian $\hat{H}_S$ must be performed. Without this approximation, no closed form for the electrical current can be obtained. Let us assume that $\hat{H}_S$ can be separated into two terms:

$$\hat{H}_S = \hat{H}_{mf} + \hat{V}_S. \tag{2.23}$$

Here, $\widehat{\mathrm{H}}_{\mathrm{mf}}$ is a single electron Hamiltonian at most experiencing the mean field of other electrons in the presence of the ions that do not belong to the nano-scale junction. $\widehat{\mathrm{V}}_{\mathrm{S}}$ represents the interaction energy between electrons beyond the mean field in the nanojunction, and the interaction energy of these electrons with the ions of the junction.

So far, all of the operators have been defined independent of the basis. However, it is desirable to calculate every quantity in terms of position (e.g. the current is derived from a surface integration of the current density). Therefore, the position representation of the operators is a good choice. In the position representation, the basis consists of an infinite set of vectors $\{|\mathbf{r}\rangle\}$, which are eigenstates of the position operator $\widehat{\mathrm{R}}$. Thus, the position representation of the state vector, known as the wave function, is $\Psi(\mathbf{r},\mathrm{t}) = \langle\mathbf{r}|\Psi(\mathrm{t})\rangle$. The momentum operator is expressed $\widehat{\mathbf{p}} = -\mathrm{i}\hbar\nabla$. In what follows, I will assume that the single-particle Hamiltonian can be generally written as

$$\mathrm{H}_{\mathrm{S}} = \frac{1}{2\mathrm{m}}\left(\mathrm{i}\hbar\nabla + \mathrm{e}\mathbf{A}(\mathbf{r},\mathrm{t})\right)^2 + \mathrm{V}_{\mathrm{S}}(\mathbf{r},\mathrm{t}), \tag{2.24}$$

such as the Schrödinger equation is

$$\mathrm{H}_{\mathrm{S}}\Psi_{\mathrm{S}}(\mathbf{r},\mathrm{t}) = \mathrm{i}\hbar\frac{\partial}{\partial\mathrm{t}}\Psi_{\mathrm{S}}(\mathbf{r},\mathrm{t}), \tag{2.25}$$

and the current density or expectation value of the current density operator is

$$\mathbf{j} = \langle\hat{\mathbf{j}}\rangle = \frac{\hbar}{2\mathrm{im}}\left[\left(\Psi_S^*(\mathbf{r},\mathrm{t})\nabla\Psi_{\mathrm{S}}(\mathbf{r},\mathrm{t}) - \Psi_{\mathrm{S}}(\mathbf{r},\mathrm{t})\nabla\Psi_S^*(\mathbf{r},\mathrm{t})\right) - 2\mathrm{q}\mathbf{A}(\mathbf{r},\mathrm{t})|\Psi_{\mathrm{S}}(\mathbf{r},\mathrm{t})|^2\right]. \tag{2.26}$$

The potential energy $\widehat{\mathrm{V}}_{\mathrm{S}}(\mathbf{r})$ may be, for example, the sum of the Hartree energy, the exchange-correlation energy, the energy due to the electron-ion interaction, and any other possible external potential energy. It describes all these interactions for the complete electrode-nanojunction-electrode system. Here, I have also implicitly assumed that electrons scatter with static ions. By doing so I am considering only elastic scattering where the energy is conserved, while single-

particle momentum changes. This amounts to saying that the time it takes electrons to relax energy due to any inelastic interaction is much longer than the time it takes electrons to traverse the junction. Similarly for the time it takes them to relax phase, as if all the energy relaxation and all dephasing effects occur in the reservoirs. This is clearly an idealization. However, in terms of the magnitude of the total resistance considering the scattering problem as phase-coherent turns out to be not a bad approximation. The reason is that the majority of the resistance is due to elastic scattering at the nano-junction, while the inelastic component generally gives a small contribution, both from electron-phonon and electron-electron interactions [17].

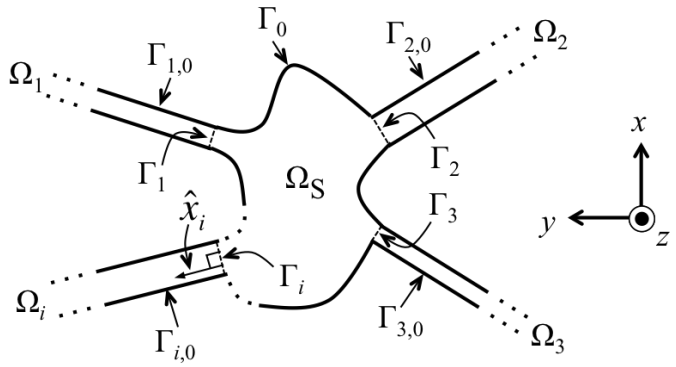

Fig. 2.2 Schematic representation of the analogy system under study. We can replace the dynamical coupling with the reservoirs with scattering boundary conditions at infinity.

C. Approximation III: Wave-Guide Boundary Conditions

Once the problem has been considered ideally stationary and H_S has been defined, the role of the reservoirs is simply to continually prepare electrons in the distant past, and far away from the nano-system, into wave-packets, which then move towards or away from the junction, without changing the current in time. Thus, the idea of solving the open quantum problem represented by an equation of the type (**2.20**) can be abandoned and instead the ¨openness¨ can be replaced with wave-guide boundary conditions. These wave-packets are now injected into the nano-system from regions of space called leads or electronic wave-guides. The waves scatter on

the nano-structure, and then move far away from it without suffering further scattering, so that they turn into different wave-packets propagating in the leads in the distant future. These are known as wave-guide boundary conditions. The system under study is now a closed but infinite system in a pure or micro-state.

A diagram that represents a z-slide of the general system under study is shown in Fig. **2.2**. The system can be divided into a "device" region Ω_S, and several waveguide or lead regions, $\Omega_1, \Omega_2, \Omega_3, \dots, \Omega_i, \dots$, which extend to infinity in the x-y plane. The boundaries of region Ω_S are $\Gamma_1, \Gamma_2, \Gamma_3, \dots, \Gamma_i, \dots$, and Γ_S, being Γ_i the boundary between the lead region Ω_i and the device region Ω_S, while Γ_S denotes the rest of its boundary. The lead boundaries are denoted $\Gamma_{i,0}$. The problem in a lead is basically two-dimensional due to the intrinsic uniformity along its length where the particle moves freely. Therefore, it is convenient to define a right-hand local coordinate system for each lead i,

$$(x_i, y_i, z_i) = [x_i(x, y, z), y_i(x, y, z), z_i(x, y, z)], \tag{2.27}$$

such that $\hat{\mathbf{x}}_i$ is the unitary vector parallel to the lead walls and points away from Ω_S. Thus, the Hamiltonian for lead i turns out to be

$$H_i = -\frac{\hbar^2}{2m}\nabla_i^2 + V_i(y_i, z_i), \tag{2.28}$$

and the corresponding time-independent Schrödinger equation,

$$H_i\Psi_i(x_i, y_i, z_i) = E\Psi_i(x_i, y_i, z_i), \tag{2.29}$$

with a general solution at a given total energy E

$$\Psi_i(x_i, y_i, z_i) = \sum_{n=1}^{N_i} a_i^n \psi_i^n(\mathbf{r}_i) + \sum_{m=1}^{N_i} b_i^m \psi_i^m(\mathbf{r}_i) + \sum_{m'=N_i+1}^{\infty} b_i^{m'} \psi_i^{m'}(\mathbf{r}_i). \tag{2.30}$$

This is the general state that one electron can occupy and consists of a linear superposition of incoming traveling-wave states,

$$\psi_i^n(\mathbf{r}_i) = \phi_i^n(y_i, z_i)e^{+ik_i^n x_i}, \tag{2.31}$$

outgoing traveling-wave states

$$\psi_i^m(\mathbf{r}_i) = \phi_i^m(y_i, z_i)e^{-ik_i^m x_i}, \tag{2.32}$$

and evanescent exponentially-decaying states

$$\psi_i^{m'}(\mathbf{r}_i) = \phi_i^{m'}(y_i, z_i)e^{-k_i^{m'} x_i}. \tag{2.33}$$

The coefficients a_i^n are an input to the problem, while the coefficients b_i^m and $b_i^{m'}$ are unknown complex numbers that must be calculated as part of the solution. The amplitude $\phi_i^o(y^i, z^i)$, taking $o = n, m$ or m', is the oth-eigenstate or transversal mode of the two dimensional Schrödinger equation

$$\left[-\frac{\hbar^2}{2m}\left(\frac{\partial}{\partial y_i} + \frac{\partial}{\partial z_i}\right) + V_i(y_i, z_i)\right]\phi_i^o(y_i, z_i) = E_i^o \phi_i^o(y_i, z_i). \tag{2.34}$$

The wave vector for the oth mode in the ith lead is given by

$$k_i^o = \sqrt{\left|(2m^*/\hbar^2)(E - E_i^o)\right|}, \tag{2.35}$$

and the number of traveling waves or transversal modes N_i allowed in the lead is the maximum m such that $E > E_i^m$. Once the transversal solutions $\phi_i^o(y_i, z_i)$ have been calculated separately, the boundary conditions at the boundaries between the system and the leads, $\Gamma_1, \Gamma_2, \Gamma_3, \ldots, \Gamma_i, \ldots$, must achieve the continuity of both the wave function and the directional derivative of the wave function,

$$\Psi_S = \Psi_i \text{ on } \Gamma_i, \tag{2.36}$$

$$\nabla\Psi_S \cdot \hat{x}_i = \nabla\Psi_i \cdot \hat{x}_i \text{ on } \Gamma_i. \tag{2.37}$$

D. Current per Mode

Lets now calculate the current through a given cross sectional surface along the lead i. For this, the current density (i.e. the expectation value of the current density operator) with only the paramagnetic component for the general state Ψ_i can be stated as

$$\mathbf{j}_i(E) = \langle \hat{\mathbf{j}}_i(\mathbf{r}_i) \rangle = \langle \Psi_i(\mathbf{r}_i) | \hat{\mathbf{j}}_i | \Psi_i(\mathbf{r}_i) \rangle = \frac{ie\hbar}{2m} [\Psi_i(\mathbf{r}_i) \nabla_i \Psi_i^*(\mathbf{r}_i) - \Psi_i^*(\mathbf{r}_i) \nabla_i \Psi_i(\mathbf{r}_i)]. \tag{2.38}$$

I then integrate the current density over a plane perpendicular to the x^i direction to calculate the average current

$$I_i(E) = \int_S \hat{\mathbf{x}}_i \cdot \mathbf{j}_i \, dS = \frac{ie\hbar}{2m} \int_{-\infty}^{+\infty} \int_{-\infty}^{+\infty} \left[\Psi_i(\mathbf{r}_i) \frac{\partial \Psi_i^*(\mathbf{r}_i)}{\partial x_i} - \Psi_i^*(\mathbf{r}_i) \frac{\partial \Psi_i(\mathbf{r}_i)}{\partial x_i} \right] dy_i \, dz_i. \tag{2.39}$$

Consider a two-port system that consists of two leads (i.e. $i = 1$ and $i = 2$) connected to a nano-structure. Consider now an electron in lead 1 in an initial eigenstate $\psi_1^n(\mathbf{r}_1)$ of H_1 with momentum $\hbar k_1^n$ such that $E = E_1^n + (\hbar k_1^n)^2/(2m)$. At the nano-system Ω_S, this state may be very complicated, according to the form of the potential energy $V_S(\mathbf{r})$. Nonetheless, a linear combination of N_1 reflected eigenstates of H_1 is reflected back into lead 1 in addition to $\psi_1^n(\mathbf{r}_1)$ after scattering at the nano-structure,

$$\Psi_1^n(\mathbf{r}_1) = \psi_1^n(\mathbf{r}_1) + \sum_{m=1}^{N_1} b_1^{mn} \psi_1^m(\mathbf{r}_1). \tag{2.40}$$

Deep into lead 2, a linear combination of N_2 eigenstates of H_2 is transmitted into lead 2

$$\Psi_2^n(\mathbf{r}_2) = \sum_{m=1}^{N_2} b_2^{mn}\psi_2^m(\mathbf{r}_2). \tag{2.41}$$

The superscripts mn indicate that the coeficients b_1^{mn} and b_2^{mn} of the reflected and transmitted states, respectively, result from the injected particle in the state $\psi_1^n(\mathbf{r}_1)$. The contribution of evanescent modes was neglected because they do not carry any current. The application of (**2**.**39**) to (**2**.**40**) and (**2**.**41**), respectively, leads to

$$I_1^E(E) = I_1^n(E) + \sum_{m=1}^{N_1} b_1^{mn} I_1^m(E) = I_1^n(E)\left[1 - \sum_{m=1}^{N_1} R_{mn}(E)\right], \tag{2.42}$$

and,

$$I_2^E(E) = \sum_{m=1}^{N_2} b_2^{mn} I_2^n(E) = I_1^n(E) \sum_{m=1}^{N_2} T_{mn}(E). \tag{2.43}$$

The reflection probability for a wave-state incident on the nano-structure with momentum $\hbar k_1^n$ to be scattered back into the same lead 1 in a state with momentum $\hbar k_1^m$, while the energy is conserved, is

$$R_{mn}(E) = |b_1^{mn}|^2 \frac{|I_1^m(E)|}{|I_1^n(E)|}. \tag{2.44}$$

Similarly, the transmission probability that the wave with initial momentum $\hbar k_1^n$ is transmitted across the nanojunction into lead 2 in a final state with momentum $\hbar k_2^m$, at the same energy, is

$$T_{mn}(E) = |b_2^{mn}|^2 \frac{|I_2^m(E)|}{|I_1^n(E)|}. \tag{2.45}$$

I have defined the current carried by each mode independently as

$$I_1^n(E) = \frac{ie\hbar}{2m}\int_{-\infty}^{+\infty}\int_{-\infty}^{+\infty}\left[\psi_1^n\frac{\partial[\psi_1^n]^*}{\partial x_1} - [\psi_1^n]^*\frac{\partial\psi_1^n}{\partial x_1}\right]dy_1\,dz_1 = e\frac{\hbar k_1^n}{m}, \tag{2.46}$$

$$I_1^m(E) = -e\frac{\hbar k_1^m}{m}, \tag{2.47}$$

and,

$$I_2^m(E) = e\frac{\hbar k_2^m}{m}. \tag{2.48}$$

Imposing the steady state condition, the current in lead 1 must be identical to the current in lead 2. Thus, expression (**2.42**) must be equal to (**2.43**) stating the conservation of particle flux as

$$\sum_{m=1}^{N_2} T_{mn}(E) + \sum_{m=1}^{N_1} R_{mn}(E) = 1. \tag{2.49}$$

E. Approximation IV: Independent-Channel Assumption

If the channels are assumed independent, the total current in the system is the sum of the current carried by all particles each in a different state. It is thus needed to multiply the one particle current $I_1^E(E) = I_2^E(E)$ by the number of states in an infinitesimal energy range dE (i.e. $D_1^n(E)dE$), to integrate in energy and to sum over all the N_1 incident channels. Since each channel represents a one-dimensional problem, the density of states for a momentum k_1^n (considering the spin of the electron) is simply

$$D_1^n(E) = \frac{Spin}{2}\left(\frac{m}{2\pi\hbar^2 k_1^n}\right). \tag{2.50}$$

Then, the current generated by channel n in the energy range dE is

$$I_1^{dE}(E) = D_1^n(E)I_2^E(E)dE = D_1^n(E)I_1^n(E)\left(\sum_{m=1}^{N_2} T_{mn}(E)\right)dE. \tag{2.51}$$

The channels are populated according to the Fermi-Dirac statistics, $F(E, E_F) = 1/\left(e^{(E-E_F)/E_T} + 1\right)$, that applies to identical non-interacting particles with half-integer spin in a system in thermodynamic equilibrium. Thus, multiplying (**2**.**51**) by the Fermi function corresponding to lead 1, $F_1\left(E, E_1^F\right)$, and integrating over all energies, the one-channel current in lead 1 is:

$$I_1^{E_F^1}(E) = \int_{-\infty}^{+\infty} F_1\left(E, E_1^F\right)D_1^n(E)I_1^n(E)\left(\sum_{m=1}^{N_2} T_{mn}(E)\right)dE_i \tag{2.52}$$

An important result of mesoscopic physics is that the density of states times the current, both corresponding to one specific transmission channel, is constant:

$$D_1^n(E)I_1^n(E) = \frac{e}{\pi\hbar}. \tag{2.53}$$

Adding the contribution of all incident channels, the total current in lead 1 is:

$$I_1^{total}(E) = \sum_{n=1}^{N_1} I_1^{E_F^1}(E) = \frac{e}{\pi\hbar}\int_{-\infty}^{+\infty} F_1\left(E, E_1^F\right)\mathcal{T}_1(E)\,dE \tag{2.54}$$

where the total transmission coefficient is

$$\mathcal{T}_1(E) = \sum_{n=1}^{N_1}\sum_{m=1}^{N_2} T_{mn}(E) \tag{2.55}$$

Similarly, the total current in lead 2 is

$$I_2^{total}(E) = \frac{e}{\pi\hbar}\int_{-\infty}^{+\infty} F_2\left(E, E_2^F\right)\mathcal{T}_2(E)\,dE \tag{2.56}$$

Finally, due to time-reversal invariance the above relations must hold even if we revert the velocities of initial and final states, by changing simultaneously the directionality of the scattering process. Then, the total transmission probabilities in lead 1 and 2 are equal,

$$\mathcal{T}_1(E) = \mathcal{T}_2(E), \tag{2.57}$$

and the total current in the system, known as the Landauer formula, can be expressed as

$$I_{total}(E) = Tr\left(\hat{\rho}_S^{ss}\hat{I}\right) = \frac{e}{\pi\hbar}\int_{-\infty}^{+\infty}\left[F\left(E, E_F^1\right) - F\left(E, E_F^2\right)\right]\mathcal{T}(E)dE \tag{2.58}$$

Where the Fermi levels and the externally applied voltage V are related to each other according to

$$eV = E_F^1 - E_F^2 \tag{2.59}$$

V. Conclusions

The determination of the current in a nano-structure is reduced to the calculation of the total transmission coefficient $\mathcal{T}(E)$ which is equivalent to solve the Schrödinger equation with wave-guide boundary conditions. Two popular procedures to solve it are the Quantum Transmitting Boundary Method [18] and the Green's Function Method [19]. In the next chapter, an analogy between the Schrodinger and Maxwell equations that show direct equivalence between the quantum transmission probability and the S-parameters calculated from full wave simulations will be demonstrated.

CHAPTER 3:
Analogy Between Maxwell and Schrödinger Equations Valid for Two-Dimensional Systems with Wave-Guide Boundary Conditions

A time-independent Maxwell-Schrödinger equation analogy is carried out for two-dimensional systems with wave-guide (lead) boundary conditions. On the lead boundaries, the third-order boundary conditions for the electric field reduce to the normal derivative of its z-component, adopting the same form of the equivalent boundary conditions for the Schrödinger equation. The total energy and position-dependent potential energy are included in the set of quantities that have an equivalent electromagnetic parameter. Standard electromagnetic analysis methods were applied to determine the wave function and transmission probability of phase-coherent quantum electron devices including a tunneling structure. The Schrödinger equation was solved via the Quantum Transmitting Boundary method for comparison with the electromagnetic simulations.

The remarkable similarities between the time-independent Schrödinger equation and the Helmholtz equation (i.e. the time-independent form of Maxwell equations) have led to de design of many new quantum electron devices where standard electromagnetic analysis techniques have been applied to study the interference, propagation, reflection, refraction and diffraction of electron waves [20]. Exact quantitative electromagnetic analogies exist for all forms of the general Hamiltonian [21], which applies to single-band effective-mass electron wave propagation in semiconductors. It has been further shown that these analogies are valid for propagation in the bulk, propagation through an interface between dissimilar materials, and propagation within one- and two-dimensional (2-D) inhomogeneous materials [22,23]. The position-dependent potential energy has been included approximately as a quantity with an equivalent electromagnetic parameter in the case of 2-D closed systems by imposing bound states in the third dimension [24].

The purpose of this thesis is to extend the previous analogy applicable to two-dimensional inhomogeneous systems adding the possibility of having current-carrying states or propagation modes via wave-guide boundary conditions. For the first time, the total energy and position-dependent potential energy are incorporated in the set of quantities with an equivalent electromagnetic parameter by direct comparison between electron waves propagating in a semiconductor heterostructure and electromagnetic waves traveling across plasma. This analogy represents an alternative approach to compute the wave function for arbitrarily shaped device regions with intricate internal potentials [25] and is suitable for the calculation of the quantum transmission probability, through the determination of the S-parameters from full-wave electromagnetic simulations. The transmission probability is frequently used to calculate the total current when electrons are coherent over the device region via Landauer-like formulas [19,17].

Section I of this chapter presents the schematic diagram of the system where the analogy will be developed. The governing electromagnetic equation and the corresponding boundary conditions will be presented in Sec. II. The analogy will be stated in Sec. III, after the quantum equivalent equation and boundary conditions are presented. A resonant cavity and a tunneling resonant structure are presented in Sec. V as examples of the application of this analogy. Section V states the corresponding conclusions.

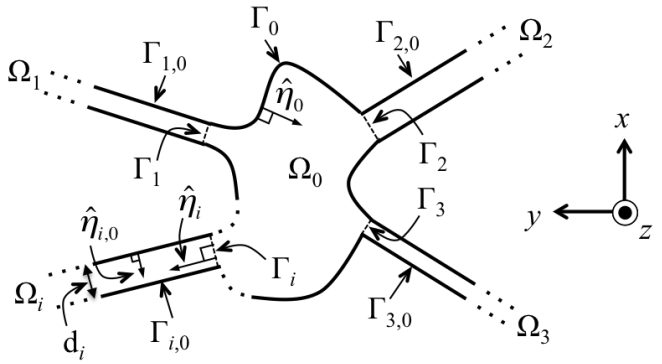

Fig. 3.1 Schematic representation of the analogy system under study.

I. The Study Case

A diagram that represents the general system where the analogy is shown to be valid is depicted in Fig. **3**.**1**. The system is assumed to be homogeneous in the z-direction. Besides, the system can be divided into a "device" region Ω_0, and several parallel-plate waveguide or lead regions, $\Omega_1, \Omega_2, \Omega_3, \dots, \Omega_n$, which extend to infinity in the x-y plane. The boundaries of region Ω_0 are Γ_i, being $\Gamma_1, \Gamma_2, \Gamma_3, \dots, \Gamma_n$ the boundaries between a lead region, Ω_i, and the device region, Ω_0, while the rest of its boundary is denoted Γ_0. The lead boundaries are denoted $\Gamma_{i,0}$.

II. Electromagnetic Case

A. Electromagnetic formulation

Consider the problem illustrated in Fig. **3**.**1**, and assume that only E_z-polarized waves are injected by the leads into de device region. Then, the scattered and total electric field will have only a z-component due to the uniformity of the structure in the z-direction. In other words, if the normal vector to the boundary surface ($\hat{n}_0$ and $\hat{n}_{i,0}$), the gradient of the permittivity and the wave number of the E_z-polarized incident waves are all contained in the x-y plane, then, the scattered waves will be E_z-polarized and will have a wave number contained in the x-y plane as well. Hence, from the time-harmonic Maxwell equations with no free charges and currents, for a homogeneous permeability, μ, and for a position dependent permittivity, $\epsilon(x,y)$, the scalar Helmholtz equation for the electric field that corresponds to the system of Fig. **3**.**1** can be expressed as

$$(\nabla^2 + \mu\epsilon(x,y)\omega^2)\, E_{z,i}(x,y) = 0, \qquad (x,y) \in \Omega_i, \tag{3.1}$$

such that

$$E_{z,0} \in C^2(\Omega_0), E_{z,1} \in C^2(\Omega_1), \dots, E_{z,n} \in C^2(\Omega_n)\,, \tag{3.2}$$

and the system has ideal conductive walls,

$$E_{z,0} = 0 \text{ on } \Gamma_0, \tag{3.3}$$

$$E_{z,i} = 0 \text{ on } \Gamma_{i,0}. \tag{3.4}$$

It is also required that the permittivity $\epsilon(x, y)$ in each lead be independent of the distance along the lead (i.e. this known as a waveguide or lead). We can choose ϵ to be frequency-dependent and to have the following form (e.g. the effective permittivity of a plasma [26]):

$$\epsilon = \epsilon_0 \left(1 - \frac{{\omega_p}^2}{\omega^2}\right), \tag{3.5}$$

where

$$\omega_p = \sqrt{\frac{ne^2}{\epsilon_0 m}} \tag{3.6}$$

is the plasma frequency, n is the density of electrons, ϵ_0 is the vacuum permittivity, e is the electron charge and m_e its mass. Therefore, when the angular frequency of the wave, ω, falls below the plasma frequency, ω_p, the wave number becomes imaginary which indicates that the wave attenuates exponentially as it propagates, in analogy to quantum tunneling. Hence, ${\omega_p}^2$ can play the role, in the Helmholtz equation for the electric field, of the potential energy, in the Schrödinger equation. Then, the larger the concentration of particles is, the higher the potential energy barrier is. An absence of particles corresponds to a null barrier.

B. Wave-guide boundary conditions

The goal is to formulate a boundary condition on the lead boundaries, $\Gamma_{i>0}$, that would allow us to specify the incoming flux in each lead and to solve the Helmholtz

equation for E_z in the device region Ω_0. This is known as wave-guide ports. At these boundaries we require both, continuity of the electric field,

$$E_{z,0} = E_{z,i} \text{ on } \Gamma_i, \tag{3.7}$$

and that the third-order boundary condition be satisfied [27],

$$\hat{n}_i \times \nabla \times E_0 = \hat{n}_i \times \nabla \times E_i \text{ on } \Gamma_i. \tag{3.8}$$

Equation (**3.8**), under the assumptions that led to Eq. (**3.1**), reduces to the continuity of the normal derivative of the z-component of the electric field:

$$\nabla E_{z,0} \cdot \hat{n}_i = \nabla E_{z,i} \cdot \hat{n}_i \text{ on } \Gamma_i. \tag{3.9}$$

$E_{z,i}$ can be expressed as a sum of traveling and evanescent modes in the leads whose amplitudes are to be determined as part of the problem's solution.

III. Quantum Case and the Analogy

The equivalent time-independent Schrödinger equation corresponding to the structure of Fig. **3.1** is

$$\left[\nabla^2 + (2m^*/\hbar^2)\big(E - V(x,y)\big)\right]\psi_i(x,y) = 0, \qquad (x,y) \in \Omega_i, \tag{3.10}$$

such that

$$\psi_0 \in C^2(\Omega_0), \psi_1 \in C^2(\Omega_1), \dots, \psi_n \in C^2(\Omega_n). \tag{3.11}$$

The corresponding boundary conditions at the hard walls $(V \to \infty)$ and at the wave-guide boundaries are:

$$\psi_0 = 0 \text{ on } \Gamma_0, \tag{3.12}$$

$$\psi_i = 0 \text{ on } \Gamma_{i,0}, \tag{3.13}$$

$$\psi_0 = \psi_i \text{ on } \Gamma_i, \tag{3.14}$$

$$\nabla\psi_0 \cdot \hat{n}_i = \nabla\psi_i \cdot \hat{n}_i \text{ on } \Gamma_i. \tag{3.15}$$

TABLE I. Analogous parameters for the quantum/electromagnetic wave propagation

QUANTUM	ELECTROMAGNETIC
E	ω^2
$V(x,y)$	$\omega_p(x,y)^2$
m^*	$\hbar^2\epsilon_0\mu/2.$

Now, since the form of the governing equations (Eq. (**3**.**1**) and Eq. (**3**.**10**)) and their respective boundary conditions (Eqs. (**3**.**3**), (**3**.**4**), (**3**.**7**) and (**3**.**9**), and Eqs. (**3**.**12**)-(**3**.**15**)) for the device and lead regions are the same, the Maxwell-Schrödinger analogy for two-dimensional systems with wave-guide boundary conditions is fully valid. The resulting set of analogies is presented in Table I.

IV. Examples

Two representative examples are presented to illustrate the analogy. The first one consists of a resonant cavity in a waveguide. The corresponding geometry is shown in Fig. **3**.**2**. The potential energy and its electromagnetic counterpart inside the device and lead regions are null. Fig. **3**.**3** and Fig. **3**.**4** show the wave function and the electric field calculated via the quantum transmitting boundary method (QTBM) [18] and calculated with Comsol Multiphysics [28], respectively. The solutions were calculated for an incident wave coming from the left with an energy $E/E_1 = 5.8$ in the first propagation mode of the waveguide. E_1 is the onset energy of the first transversal mode. A comparison between the transmission coefficient, T, (solved via the QTBM) and the squared magnitude of the S21-parameter (solved

with Comsol) as a function of energy for the first transmission mode is shown in Fig. **3**.**5**.

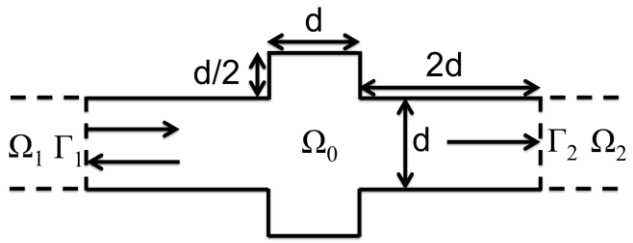

Fig. 3.2 The scattering geometry

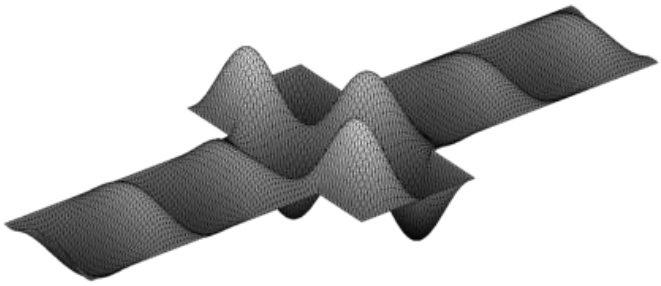

Fig. 3.3 Wave function, calculated via the QTBM, for an incident wave in the first propagation mode with a normalized energy of $\mathrm{E}/\mathrm{E}_1 = 5.8$.

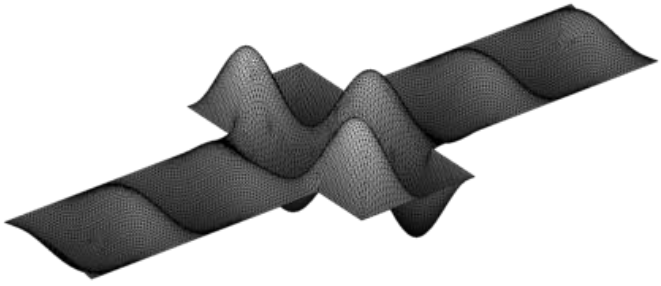

Fig. 3.4 Electric field, solved with Comsol, for an incident wave in the first propagation mode with an equivalent normalized energy of $\mathrm{E}/\mathrm{E}_1 = 5.8$.

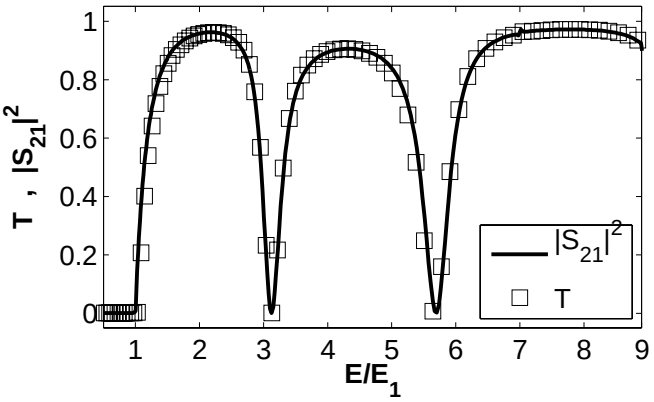

Fig. 3.5 A comparison between the transmission, T, (via the QTBM) and the squared magnitude of the S21-parameter (via Comsol).

The second example consists of a resonant tunneling structure in a waveguide. The corresponding geometry is shown in Fig. **3**.**6**. Note that two potential barriers were added. Fig. **3**.**7** and Fig. **3**.**8** show the wave function and the electric field calculated via the QTBM and calculated with Comsol Multiphysics, respectively. The solutions were calculated for an incident wave coming from the left with an energy $\mathrm{E}/\mathrm{E}_2 = 3.88$ (the resonant tunneling peak) in the second propagation mode of the waveguide. E_2 is the onset energy of the second transversal mode. A comparison between the transmission coefficient, T, (solved via the QTBM) and the squared magnitude of the S21-parameter (solved with Comsol) as a function of energy for the second transmission mode is shown in Fig. **3**.**9**.

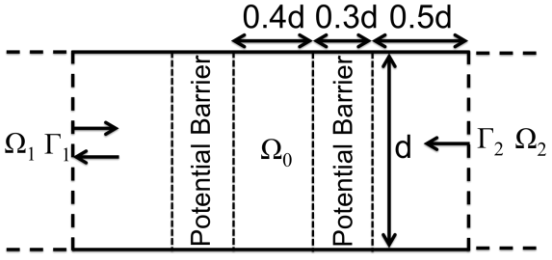

Fig. 3.6 The scattering geometry.

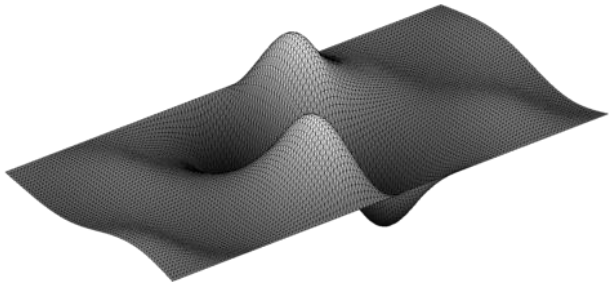

Fig. 3.7 Wave function, calculated via the QTBM, for an incident wave in the first propagation mode with a normalized energy of $\mathrm{E}/\mathrm{E}_2 = 3.88$.

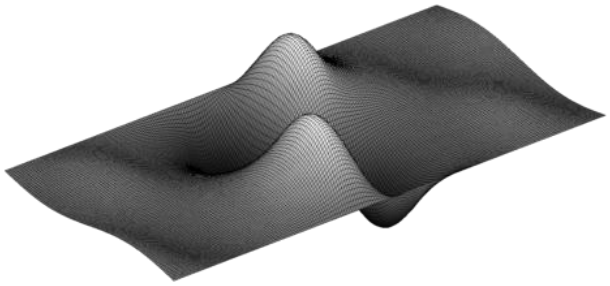

Fig. 3.8 Electric field, solved with Comsol, for an incident wave in the first propagation mode with an equivalent normalized energy of $\mathrm{E}/\mathrm{E}_2 = 3.88$.

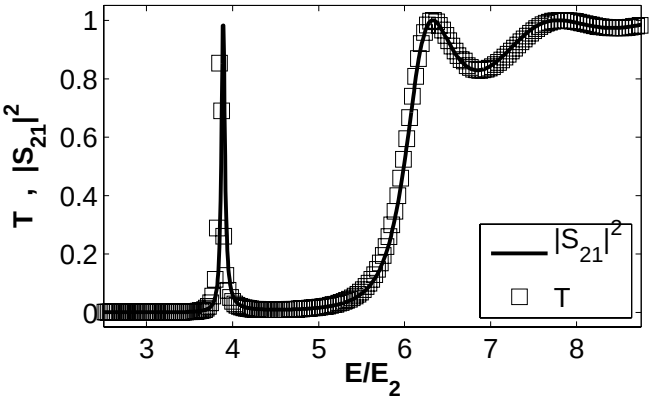

Fig. 3.9 A comparison between the transmission, T, (via the QTBM) and the squared magnitude of the S21-parameter (via Comsol).

V. Conclusions

An analogy between the time-independent form of the Maxwell equations and the time-independent effective-mass Schrödinger equation was presented. It was proved that this analogy is valid for two-dimensional systems with wave-guide boundary conditions and introduced two examples that illustrate the analogy. This analogy, when fulfilled, is an alternative strategy to calculate the wave function without actually solving the Schrödinger equation, and it might represent an advantage when full wave simulation software is available. In addition, the calculations introduced in this work are applicable to the study of carrier transport in a large variety of quasi 2-D semiconductor structures, where electrons are coherent over the device region due to its small dimensions, a condition that is reinforced when the device is operated at low temperatures or exposed to a high magnetic field.

CHAPTER 4:
Multiport Analysis of Two-Dimensional Nanosystems in a Magnetic Field Based on the NEGF Formalism

When full quantum mechanical characterization and modeling of charge carrier transport in nano-scaled semiconductor devices is required, the Non-Equilibrium Green's Function (NEGF) formalism is the most prominent theoretical approach now days. In fact, the NEGF formalism is considered the quantum version of the Boltzmann transport theory. Based on this theory, a systematic analysis of different multiport nanostructures modulated by the action of a magnetic field is introduced in this chapter.

With the purpose of improving device performance and increase integration density, modern transistors are down scaled to a 10 nm size and below. At these device dimensions, electrons (or holes) travel from source to drain without suffering inelastic scattering. Under this condition, the dynamics of the carriers in the channel is deterministic and is represented by the Schrodinger equation. The Non-Equilibrium Green's Function (NEGF) formalism provides an efficient manner to impose the appropriate boundary conditions needed to solve the Schrodinger equation. Therefore, the NEGF formalism can be used to analyze the wave nature of the carrier transport in a large variety of nano-scaled semiconductor devices.

There is a variety of nano-scaled MOSFET models. However, many of them apply semi-classical approaches that treat the electrons only as particles, neglecting the possible phenomena resulting of the wave nature of the electrons [29,30]. Some models include the influence of a magnetic field classically, which is incorrect at high field intensities [31]. Other descriptions consider only two ports or include the influence of another port by post-processing the resulting two ports data [32]. There are quantum models of one-dimensional nanostructures [33,34], but in this case the charges cannot be deflected by a magnetic field. Therefore, a multiport analysis that uses a magnetic field as an auxiliary modeling tool, will render in the development of

a wave-nature new transistor model, very much required for the new sub 10 nm scale era.

A systematic analysis of representative nanostructures shows the non-ohmic behavior of nano-systems under different electrical bias conditions. In addition, extreme cases in the analysis that agree with the theory of quantum transport are introduced as a way to validate the results.

The rest of this chapter is organized as follows: Section I briefly describes the NEGF formalism. Section II shows the quantum transport analysis of one-dimensional systems, and Section III extends the analysis to bi-dimensional multiport structures under the influence of a magnetic field and shows the simulation results.

I. NEGF Formalism.

The kind of devices analyzed in this chapter is the one composed by reservoirs and baths that surround and perturb the nano-structure of interest in the way explained in chapter 2. A reservoir is a subsystem that is assumed to remain in local equilibrium all the time and that can exchange particles with the nanostructure. A bath is a subsystem that only exchanges energy but not particles. The transistor belongs to this category since the source and drain contacts constitute the reservoirs, the ideal gate is the bath that is able to induce an electric field and the channel is the nano-structure of interest. In this case, it is said that the channel is open to the contacts. It must be emphasized that the analysis will include only elastic scattering inside the channel and that all the heat dissipation occurs in the contacts.

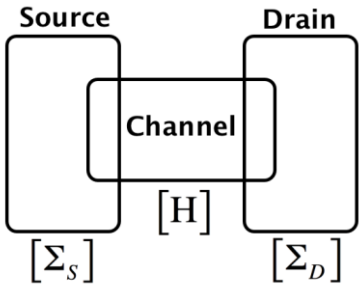

Fig. 4.1 Schematic view of the channel coupled to the contacts.

An open system, like the transistor, is mathematically described by the Hamiltonian of the channel H and the self-energies corresponding to the source and drain contacts (Σ_S, Σ_D) [35]. The Hamiltonian represents the dynamics of the charge carriers inside the channel (kinetic and potential energy) and the self-energies represent the level of coupling between the contacts and the channel (see Fig. **4.1**). In fact, the self-energies play the role of the leads in chapter 2. The time-independent Schrödinger equation for one particle corresponding to an open system is (in matrix form):

$$[\mathrm{EI} - \mathrm{H} - \Sigma_S - \Sigma_D]\{\Psi\} = \{S\} \tag{4.1}$$

Where E is the total energy; I is the identity matrix of the same size as the Hamiltonian of the isolated channel H; Ψ is the wave function and S corresponds to an external perturbation (current and voltage probes). This equation is the discrete version of a non-homogeneous differential equation.

The Hamiltonian of the isolated channel including the electromagnetic fields is:

$$\mathrm{H} = \frac{1}{2\mathrm{m}}\left(\mathrm{i}\hbar\nabla + \mathrm{e}\mathbf{A}(\mathbf{r})\right)^2 + \mathrm{U}(\mathbf{r}), \tag{4.2}$$

where $\mathbf{A}$ and U are the vector and scalar potentials that correspond to the electromagnetic field and m is the electron mass. The system Hamiltonian H by itself represents a closed system and does not describe the in and out flux of electrons from the channel. On the other hand, $[\mathrm{EI} - \mathrm{H} - \Sigma_S - \Sigma_D]$ can be considered as an effective Hamiltonian that allows the desired charge flux to occur when the appropriate boundary conditions are imposed by the contacts (i.e. wave-guide boundary conditions). The energy dependent quantities Σ_S and Σ_D can be numerically determined by a recursive procedure [19].

Since this work focuses on determining macroscopic observables such as the current, it is important to determine the probability that an electron injected from a contact into the channel has to be transmitted to the other contact. The transmission probability is defined as:

$$T = \mathrm{Trace}\left[\Gamma_S G \Gamma_D G^{\dagger}\right] \tag{4.3}$$

where

$$\Gamma_S = i\left[\Sigma_S - \Sigma_S^{\dagger}\right] \ , \ \Gamma_D = i\left[\Sigma_D - \Sigma_D^{\dagger}\right] \tag{4.4}$$

and

$$G = [EI - H - \Sigma_S - \Sigma_D]^{-1}. \tag{4.5}$$

Note that G is the Green's function of the open system and $(\dagger)$ represents the conjugate transpose operator. Finally, the equation for calculating the current as a function of the transmission is (**2**.**58**):

$$I(E) = \frac{e}{\pi\hbar}\int_0^{\infty}\left[F\left(E, E_F^S\right) - F\left(E, E_F^D\right)\right]\mathcal{T}(E)dE, \tag{4.6}$$

where $F\left(E, E_F^S\right)$ and $F\left(E, E_F^D\right)$ the Fermi functions of the source and drain contacts

$$F(E) = \left(e^{-\frac{E-E_F^S}{k_B T}} + 1\right)^{-1}, F(E) = \left(e^{-\frac{E-E_F^D}{k_B T}} + 1\right)^{-1} \tag{4.7}$$

with electrochemical potentials E_F^S and E_F^D, respectively. k_B and T are the Boltzmann constant and the temperature, respectively.

II. One-Dimensional Analysis (B=0)

The band diagram or potential profile $U(x)$ versus position of a 65 nm n-MOSFET under different polarization voltages is depicted in Fig. **4**.**2**. At low gate voltages, the energy barrier between the source and drain is high, and the device is off. A high drain bias lowers the energy in the drain, and when a high gate voltage lowers the

potential energy barrier, electrons flow from source to drain. Then, transistor action occurs by modulating the height of the energy barrier.

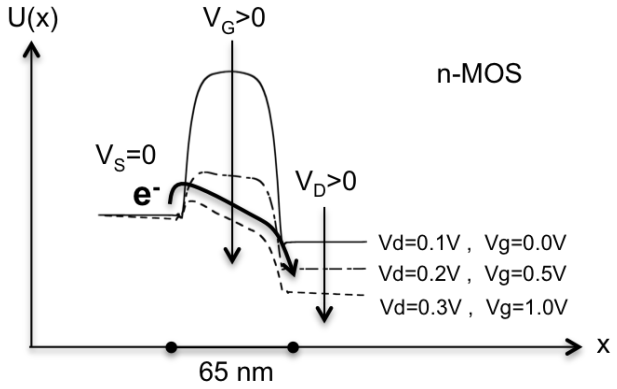

Fig. 4.2 Simulated energy band diagrams or a 65 nm n-MOS transistor under different drain and gate voltages. Simulations were performed with Minimos NT [36].

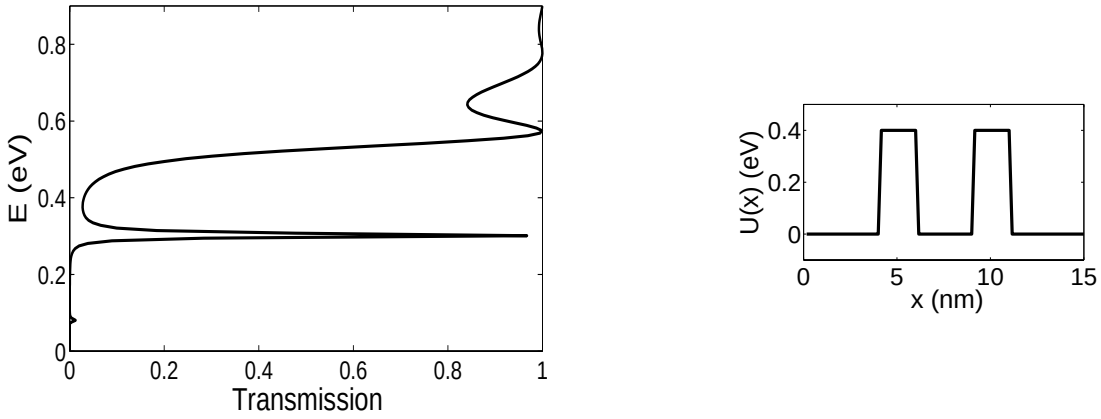

Fig. 4.3 Left: electron transmission probability as a function of energy for electron motion across the double-barrier structure. Right: potential profile versus position.

The result of considering the wave nature of electrons in the form of quantum-wave states is clearly visible in the double potential-barrier structure (see right plot in Fig. **4.3**) where a resonance can be seen in the transmission coefficient (see left plot in Fig. **4.3**) as well as in the current-voltage characteristics shown in

Fig. **4.4**. Note that electrons with energy $E = 0.3\,eV$ have a unity transmission probability. The effective mass of the gallium arsenide at room temperature for all the simulations in this chapter was implemented.

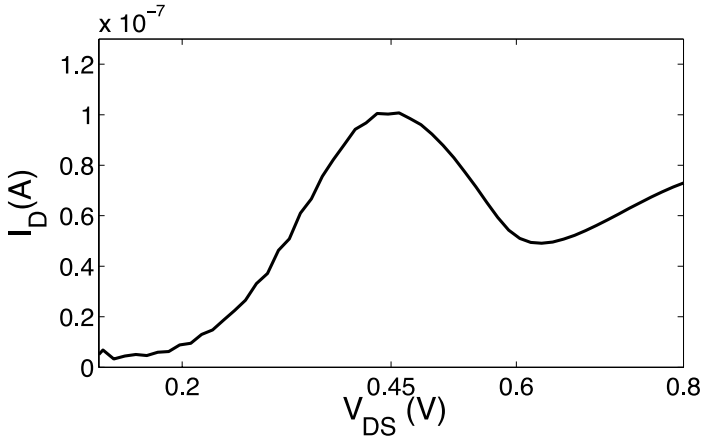

Fig. 4.4 Drain current (I_D) versus drain-source voltage (V_{DS}) to a double-barrier structure.

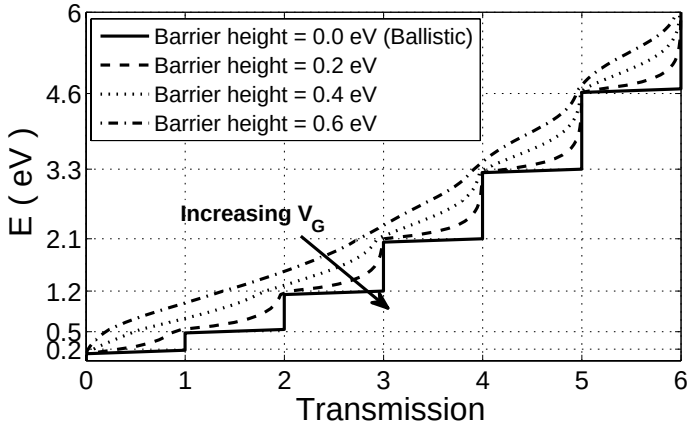

Fig. 4.5 Transmission of a two-dimensional structure for different barrier heights.

III. Two-Dimensional Analysis

The presence of transversal modes in a two-dimensional system gives place to discrete sub-bands or transmission modes separated from each other by an energy

gap. Hence, more than one electron with the same total energy can be transmitted simultaneously in analogy with an electromagnetic waveguide where different propagation modes can coexist. In order to save simulation time, the chosen structure to be analyzed is simple and small. The structure is a nanowire of 6 nm wide and 15 nm long.

A. Different Barrier Heights (B=0 T)

In order to visualize the activation of the different transmission modes, the simulated transmission of the nanowire under study (6 nm wide and 15 nm long) is shown in Fig. **4.5**. For a null potential barrier (barrier height = 0), a ballistic transmission is obtained. The onset energies of the different transmission modes are clearly shown by the discontinuities at $\mathrm{E} = 0.2, 0.5, 1.2, 2.1, 3.3$ and $\mathrm{and}\ 4.6\ \mathrm{eV}$. Thus, one transversal mode propagates between 0.2 and $0.5\ \mathrm{eV}$; two transversal modes propagate between 0.5 and $1.2\ \mathrm{eV}$ and so on. Note that the transmission becomes continuous and lowers in magnitude in the presence of a potential barrier as expected.

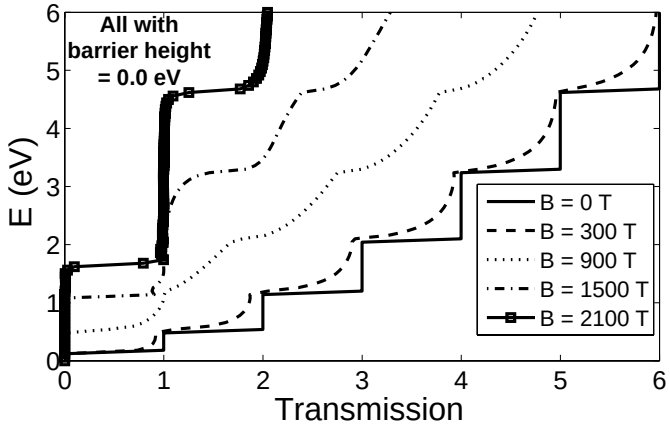

Fig. 4.6 Transmission of a two-dimensional structure for different magnetic field intensities. The potential barrier is absent for all cases.

B. Applying a Magnetic Field (B≠0 T)

The influence of a perpendicular magnetic field (normal to the surface of the two-dimensional structure) is added to the analysis. Because the structure under analysis is too small, very high intensities of a magnetic field are needed to observe its effects. Despite this, the analysis does not lack generality. For instance, in the case of a real MOSFET that has a width of 1 μm, the magnetic field intensities at which quantum phenomena become evident are relatively small (for classical effects the intensity needed is even smaller). Fig. **4.6** depicts the transmission of the quantum wire of the previous section but this time for different magnetic field intensities. The ballistic case is shown as a reference. The important thing to note is that at high enough magnetic field intensities (B = 2100 T) the transmission becomes ballistic again. This is evident from the formation of discontinuities. Fig 4.7 shows that even in the presence of a potential barrier, ballistic transmission can be achieved! This is known as the quantum Hall effect. In this regime the carrier transport is carried out near to the edges of the structure. The carrier states responsible of this are known as edge states. Besides, quantized transmission gives rise to the quantized conductance and within the quantum Hall effect regime the quantization is so precise that it has been established as an electrical resistance standard [37].

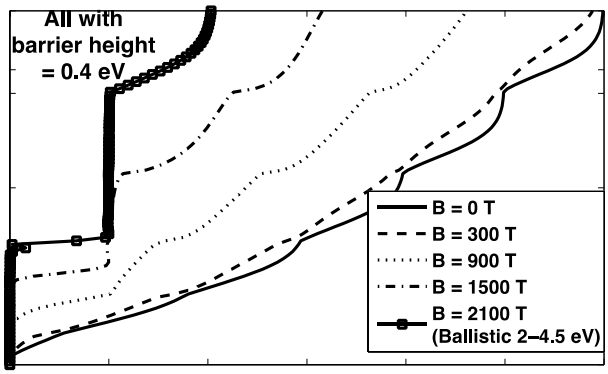

Fig. 4.7 Transmission of a two-dimensional structure for different magnetic field intensities. The height of the potential barrier is 0.4 eV in all cases.

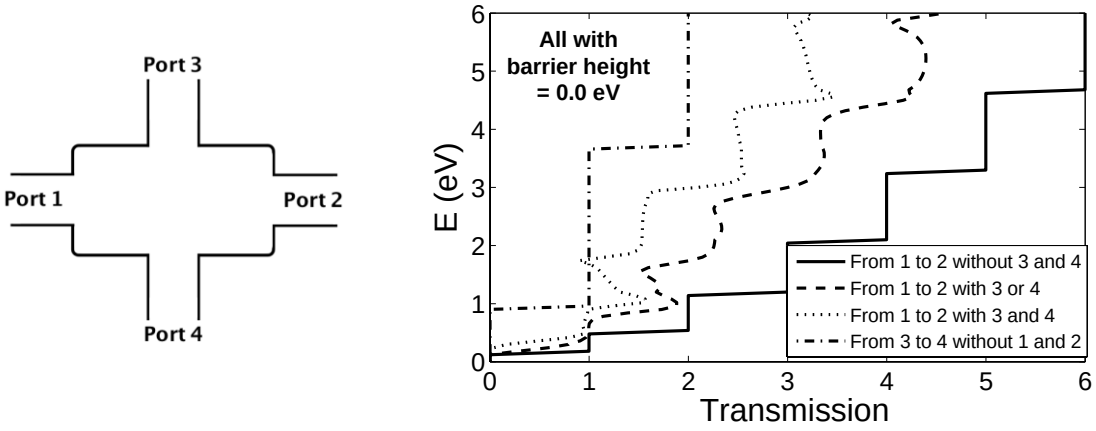

Fig. 4.8 Left: four-port two-dimensional system. Right: transmissions for the multiport two-dimensional system.

C. Multiport Analysis (B=0)

In general, the presence of active or inactive ports modifies the quantum transport properties of the device being analyzed (see the diagram Fig. **4.8**). The plot in Fig. **4.8** shows, as references, the ballistic transmission from port 1 to port 2 (from port 3 to port 4) without the presence of ports 3 and 4 (ports 1 and 2). It is interesting how the transmission from port 1 to port 2 lowers if port 3 or port 4 (ports 3 and 4) is (are) present inactively (there is not current flux across these ports).

D. Multiport Analysis Including the Magnetic Field (B≠0)

The transmission for all the systems analyzed until now is symmetric (time reverse invariant) [38]. This means that the transmission from port m to port n $\mathrm{T}(\mathrm{m} \to \mathrm{n})$ is the same as the transmission from port n to port m $\mathrm{T}(\mathrm{n} \to \mathrm{m})$,

$$\mathrm{T}(\mathrm{m} \to \mathrm{n}) = \mathrm{T}(\mathrm{n} \to \mathrm{m}). \tag{4.8}$$

However, under the presence of a magnetic field this is no longer true. In general, the only thing that can be said is

$$[\mathrm{T}(\mathrm{m} \to \mathrm{n})]_{+\mathrm{B}} = [\mathrm{T}(\mathrm{n} \to \mathrm{m})]_{-\mathrm{B}}, \tag{4.9}$$

with the only exception of the two-port system were the transmission is symmetric,

$$[\mathrm{T}(1 \to 2)]_{+\mathrm{B}} = [\mathrm{T}(1 \to 2)]_{-\mathrm{B}}. \tag{4.10}$$

The MOSFET can be considered as a three-port (four-port) system if the gate is considered as a contact (if the gate and bulk have a contact). Relation (4.9) is known as the Onsager-Casimir reciprocity relation for nano-systems. Fig. **4.9** shows that the simulator developed for this analysis matches the predicted behavior by the Onsager-Casimir reciprocity relation, validating the analysis.

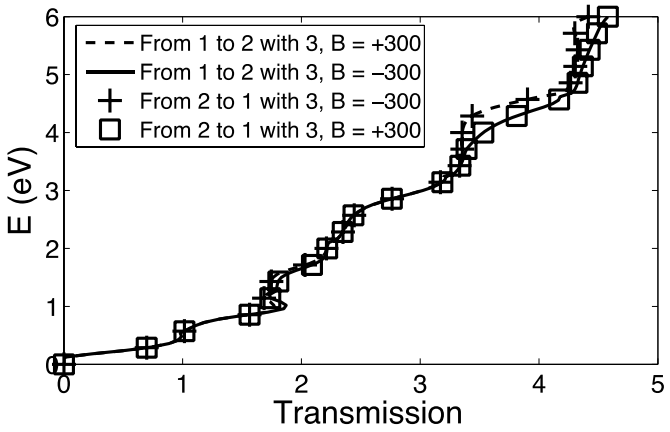

Fig. 4.9 The Onsager-Casimir reciprocity relation is matched.

E. I_D-V_G Characteristics of the 3-port 2-D System in a Magnetic Field with Opposite Directions

Fig. **4.10** shows the impact of changing the magnetic field direction to an opposite side on the drain current-gate voltage curve. The main thing to consider is that for $\mathrm{V_G} < 0.8\,V$ the respective values for $\mathrm{I_D}$ is larger for the curve corresponding to the positive magnetic field and for $\mathrm{V_G} > 0.8\,V$ the corresponding values for $\mathrm{I_D}$ are greater for the negative magnetic field.

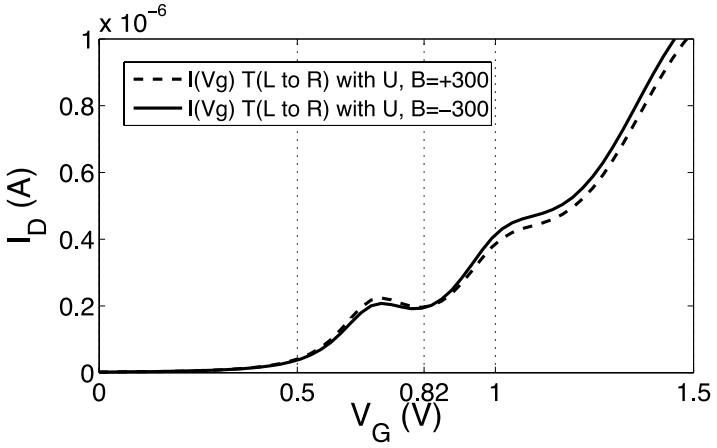

Fig. 4.10 Relationship $I_D - V_G$ of the three-port two-dimensional system in a magnetic field with opposite directions.

IV. Conclusions

A quantum analysis where the electron's wave nature was accounted for was presented for a different variety of semiconductor nanostructures. The influence of an external magnetic field as well as different potential profiles has been included, which serves as an exploratory tool to study magneto-quantum effects in nano-scaled semiconductor devices, like MOSFETs, FinFETs, nano-wires, and quantum dots. This analysis and model is expected to serve as a tool for device designers to optimize the electrical performance of nano-scaled semiconductor devices.

Articles

V. H. Vega-G., E. A. Gutiérrez-D. and F. Guarin "A Negative Differential Resistance Effect Implemented with a Single MOSFET from 375 K down to 80 K," Proceedings of the 49rd European Solid-State Device Research Conference, September 2013, Bucharest, Romania.

E. A. Gutiérrez-D., E. Póndigo-de los A., V. H. Vega-G., and F. Guarin "Observation of Asymmetric Magnetoconductance in Strained 28-nm Si MOSFETs," IEEE Electron Device Letters, Vol. 33, No. 2, February 2012.

V. H. Vega-G., E. A. Gutiérrez-D., "Multiport Analysis of Two-Dimensional Nanosystems in a Magnetic Field Based on the NEGF Formalism," Proceedings of the XVIII International IBERCHIP Workshop (IEEE), February 2012, Playa del Carmen, Mexico.

E. A. Gutiérrez-D., E. Póndigo de los A., V. H. Vega-G., and F. Guarin, "Gate Current Magneto-tunneling in Strained 28nm High-k pFETs," IEEE Semiconductor Interface Specialists Conference, December 2011, Arlington, VA.

BIBLIOGRAPHY

[1] P. R. Berger, and R. Loo A. Ramesh, "High 5.2 peak-to-valley current ratio in Si/SiGe resonant interband tunnel diodes grown by chemical vapor deposition," *Appl. Phys. Lett.*, vol. 100, 2012.

[2] R. Tsu L. Esaki, "Superlattice and negative differential conductivity in semiconductors," *IBM J. Res. Develop.*, vol. 14, no. 1, pp. 61-65, January 1970.

[3] J. P. A. Van Der Wagt, "Tunneling-based SRAM," *Proceedings of IEEE*, vol. 87, no. 4, pp. 571-595, April 1999.

[4] A. Mathewson, A. Concannon R. Duane, "Bistable gated bipolar device," *IEEE Electron Device Letters*, vol. 24, no. 10, pp. 661-663, October 2003.

[5] R. Duane X. Cheng, "A comprehensive study of bistable gated bipolar device," *IEEE Transactions on Electron Devices*, vol. 53, no. 10, pp. 2589-2597, October 2006.

[6] S. Soliveres, C. Le Royer, S. Cristoloveanu, L. Clavelier et al. A. Zaslavsky, "Negative transconductance in double-gate germanium-on-insulator field effect transistors," *Applied Physics Letters*, vol. 91, pp. 183511-32, October 2007.

[8] S.M. Sze, *Physics of Semiconductor Devices*, 2nd ed.: Wiley, 1981.

[7] S. Hall, P.H. Mellor, W. Eccleston, J.C. Alderman L.J. Mcdaid, "Explanation for the Negative Differential Resistance in SOI-MOSFETs," in *ESSDERC*, Berlin, 1989.

[9] A. W. Hull, "The dynatron—A vacuum tube possessing negative electric resistance," *Proceedings of the IRE*, vol. 6, no. 1, pp. 5-35, February 1918.

[10] J. Yu, Y. Yu L. O. Chua, "Bipolar-JFET-MOSFET negative resistance devices," *IEEE Transactions on Circuits and Systems*, vol. CAS-32, no. 1, pp. 46-61, January 1985.

[11] Ilham Hassoune, "Design and optimization of digital circuits for low-power and security applications," Catholic University of Leuven, Belgium, PhD Thesis 2006.

[12] V. Pott, D. Bouvet, M. Mazza, S. Mahapatra, A. Schmid, Y. Leblebici, M. J. Declercq, A. M. Ionescu S. Ecoffey, "Nano-wires for roomtemperature operated hybrid CMOS-NANO integrated circuits," *Proc. ISSCC Tech. Dig.*, pp. 260-597, 2005.

[13] Kwang-Jow Gan, "The Low-High-Low I V Characteristics of Five to Seven Peaks Based on Four NDR Devices," *IEEE Transactions on Electron Devices*, vol. 48, no. 8, pp. 1683-1687, August 2001.

[14] G. Ribes et al., "Review on High-k Dielectrics Reliability Issues," *IEEE*

Transaction on Device and Materials Reliability, vol. 5, no. 1, March 2005.

[15] T.Futatsugi et al., "Silicon Single-electron Memory Using Ultra-small Floating Gate," *Fujitsu Sci. Tech. J.*, vol. 34, no. 2, pp. 142-152, December 1998.

[16] W. J. Zhu et al., "Current Transpor tin Metal/Hafnium Oxide/Silicon Structure," *IEEE Electron Device Letters*, vol. 23, no. 2, February 2002.

[18] D. J. Kirkner C. S. Lent, "The quantum transmitting boundary method," *Journal of Applied Physics*, vol. 67, no. 6353, 1990.

[17] Di Ventra, *Electrical Transport in Nanoscale Systems*. UK: Cambridge, 2008.

[19] S. Datta, *Electronic Transport in Mesoscopic Systems*. UK: Cambridge, 1996.

[20] M. Dragoman D. Dragoman, *Quantum Classical Analogies*. Germany: Springer, 2004.

[21] K. R. Brownstein R. A Morrow, "Model effective-mass Hamiltonians for abrupt heterojunctions and the associated wave-function-matching conditions," *Physical Review B*, vol. 30, no. 678, July 1984.

[22] T. K. Gaylord, E. N. Glytsis G. N. Henderson, "Ballistic electron transport in semiconductor heterostructures and its analogies in electromagnetic propagation in general dielectrics," *Proceedings of the IEEE*, vol. 79, no. 11, 1991.

[23] T. K. Gaylord, E. N. Glytsis G. N. Henderson, "Electromagnetic analogies to general-Hamiltonian effective-mass electron wave propagation in semiconductors with spatially varying effective mass and potential energy," *Physical Review B*, vol. 45, no. 8404, April 1992.

[24] H.-J. Stockmann, *Quantum Chaos: an Introduction*. New York: Cambridge, 1999.

[25] et al. J. T. Londergan, *Binding and Scattering in Two-Dimensional Systems*. Germany: Springer, 1999.

[26] C. Kittel, *Introduction to Solid State Physics*, 8th ed. USA: Wiley, 2005.

[28] COMSOL Multiphysics. [Online]. www.comsol.com

[27] J. Jin, *The Finite Element Method in Electromagnetics*. New York: John Wiley and Sons, 2002.

[29] Mark S. Lundstrom et al., *Nanoscale transistors: device physics, modeling and simulation*.: Springer, 2006.

[30] Y. Tsividis, *Operation and Modeling of the MOS Transistor*, 2nd ed., McGraw-Hill, Ed. New York, 1999.

[31] R. S. Popovic, *Hall Effect Devices*, 2nd ed. UK, 2004.

[32] W.L., Holtzhausen, J.P. Vosloo, "The prediction of insulator leakage currents from environmental data," in *IEEE AFRICON*, vol. 2, 2002, pp. 603-608.

[33] P. Harrison, *Quantum Wells, Wires and Dots: Theoretical and Computational*

Physics of Semiconductor Nanostructures, 2nd ed., Willey, Ed., 2005.

[34] A. F. Levi, *Applied Quantum Mechanics*, Cambridge University Press, Ed., 2003.

[35] S. Datta, *Quantum Transport: Atom to Transistor*. New York: Cambridge, 2005.

[36] Globaltcad. [Online]. www.globaltcad.com

[38] L. I. Schiff, *Quantum Mechanics*, 3rd ed.: McGraw-Hill, 1995.

[37] Jeanneret B. Jeckelmann and B, "The Quantum Hall Effect as an Electrical Resistance Standard," *Swiss Federal Office of Metrology and Accreditation* , vol. Lindenweg 50, no. CH-3003.

[39] P.B. Klein, T.E. Kazior S.C. Binari, "Trapping Effects in GaN and SiC Microwave FETs," *Proceedings of the IEEE*, vol. 90, pp. 1048-1058, June 2002.